Green Chemistry

ROYAL SOCIETY OF CHEMISTRY

CRITICAL REVIEW

View Article Online
View Journal | View Issue

Cite this: *Green Chem.*, 2025, **27**, 15374

Aluminum–graphite dual-ion batteries: recent advances and challenges

Hui Shi, [a,b] Anastasia A. Teck, [b] Laura Lander[c] and
Maria-Magdalena Titirici *[b,d]

Received 24th September 2025,
Accepted 13th October 2025

DOI: 10.1039/d5gc05069c

rsc.li/greenchem

Aluminum–graphite dual-ion batteries (AGDIBs) are emerging as a promising alternative in electrochemical energy storage due to aluminum's abundance, low cost, intrinsic safety, high power density, and excellent performance across a wide range of temperatures. Unlike single-ion rocking-chair batteries, AGDIBs operate *via* a dual-ion mechanism: Al plating/stripping at the Al anode and $AlCl_4^-$ anions intercalation/deintercalation in the graphitic carbon cathode. Recent years have witnessed significant progress in the development of AGDIBs, particularly in anode interface engineering, graphite cathode optimization, and the formulation of novel electrolytes. Despite these advancements, critical challenges persist, including the low specific capacity of the graphitic carbon cathode and severe electrolyte-induced corrosion. This review offers a comprehensive and up-to-date analysis of recent advancements and persistent challenges in the development of AGDIBs. It systematically examines innovations across all components—including anodes, cathodes, electrolytes, and others—highlighting breakthroughs in materials design and performance optimization. Beyond summarizing progress, the review critically identifies unresolved issues and knowledge gaps, offering forward-looking insights to guide future research efforts.

Green foundation

1. We review the recent breakthroughs in aluminum–graphite dual-ion batteries (AGDIBs), emphasizing the use of Earth-abundant materials (aluminum, graphite), non-flammable ionic liquid electrolytes, and extended temperature stability. These developments reduce reliance on critical metals and improve safety and robustness in battery systems.
2. AGDIBs align with circular economy and sustainable energy goals by offering lower environmental impact, enhanced safety, and reduced resource risk compared to lithium-ion systems. As demand for green energy storage grows, AGDIBs present an attractive alternative, addressing both technical and policy imperatives.
3. We identify key challenges such as limited cathode capacity, electrolyte corrosion, and lifecycle integration. We propose targeted directions—*e.g.* novel cathode architectures, corrosion-resistant interfaces, and system-level design strategies—that can guide future R&D toward truly sustainable, high-performance AGDIB systems.

1. Introduction

Aluminum (Al) offers several unique advantages, making it a promising material for the development of sustainable metal batteries. Al exhibits notable electrochemical properties, including a high theoretical volumetric capacity of 8046 mAh cm^{-3}—approximately four times that of lithium—and a theoretical gravimetric capacity of 2980 mAh g^{-1}, second only to lithium.[1] In addition to its electrochemical advantages, Al is the third most abundant element in the Earth's crust, following oxygen and silicon, accounting for approximately 8.1% by mass.[2] Its abundance contributes to a significant cost advantage over other battery metals such as lithium and sodium, making it an attractive choice for large-scale energy storage applications. Non-aqueous aluminum-ion batteries (AIBs) typically consist of a metallic Al anode, a chloroaluminate-based ionic liquid electrolyte (commonly derived from $AlCl_3$), and a compatible cathode material. Various materials have been applied as cathodes for AIBs, such as graphitic carbon materials, organic materials, transition metal oxides, selenides, and sulfides. Among these, graphitic carbon materials are particularly attractive due to their excellent electronic conductivity and ability to reversibly intercalate $AlCl_4^-$ anions, which facilitates relatively fast redox kinetics and stable cycling performance. The batteries based on an Al anode, an

---

[a] *School of Mechanical Engineering, Chengdu University, Chengdu 610106, China*
[b] *Department of Chemical Engineering, Imperial College London, London SW7 2AZ, UK. E-mail: m.titirici@imperial.ac.uk*
[c] *Department of Engineering, King's College London, London WC2R 2LS, UK*
[d] *Advanced Institute for Materials Research, Tohoku University, Sendai 980-8577, Japan*

ionic liquid electrolyte and a graphitic carbon cathode are generally referred to as aluminum–graphite dual-ion batteries (AGDIBs).[3] Fig. 1a presents a Ragone plot of AGDIBs reported on the literature in comparison with various electrochemical energy storage systems. AGDIBs maintain a stable energy density of up to 66 Wh kg^{-1} while delivering ultrahigh power densities of up to 175 kW kg^{-1},[4] which is one to two orders of magnitude higher than those of lithium-ion, sodium-ion, and redox flow batteries, and comparable to state-of-the-art electrochemical supercapacitors.[5–8] This unique combination of steady energy density and extraordinary power capability positions AGDIBs between batteries and supercapacitors. Such attributes make them attractive for high-power applications ranging from electric vehicles and portable electronics to renewable energy storage (*e.g.*, solar and wind), as well as grid stabilization and other industrial uses where both energy efficiency and rapid power delivery are essential.

Understanding how AGDIBs function requires examining their distinct charge storage mechanism, which differs fundamentally from traditional AIBs. Unlike rocking-chair AIBs, which struggle with reversible Al^{3+} ion storage, AGDIBs operate *via* a different mechanism. In rocking-chair systems,[9–11] the energy storage relies on the reversible transfer of Al^{3+} ions and metallic aluminum between both electrodes (Fig. 1b). However, it often suffers from poor reversibility due to the trivalent ion's high charge density and sluggish kinetics. In contrast, AGDIBs belong to a class of dual-ion systems where energy storage is enabled by the shuttling of complex aluminum chloride anions between the electrolyte and the electrodes during charge and discharge. This anion-shuttling mechanism avoids the challenges associated with Al^{3+} intercalation. In AGDIBs, the electrolyte assumes a dual function: it not only mediates ion transport between the electrodes but also provides the electroactive complexes (*e.g.*, $AlCl_4^-$ and $Al_2Cl_7^-$) that directly participate in charge storage at both the anode and cathode. Currently, $AlCl_3$/1-ethyl-3-methyl-imidazolium chloride ([EMIm]Cl) is the main electrolyte applied in AGDIBs. The cell operates within 0 to 2.5 V, limited by the electrochemical stability of the chloroaluminate electrolyte and the redox potentials of the electrodes. The onset potential for Al deposition was identified at −0.25 to −0.12 V *vs.* Al/Al^{3+}, while the stripping current drops to zero between 0.8 and 1.5 V due to passivation of the aluminum electrode. Both deposition and stripping behaviors are strongly influenced by the specific electrolyte formulation.[12–14] Concurrently, at the cathode, chloroaluminate anions ($AlCl_4^-$) intercalate into graphitic carbon at an average voltage of 2.01–2.3 V,[15] leading to the formation of graphite intercalation compounds (GICs). The principle can be simply described as following equations[16] and Fig. 1b:

Anode:

$$4Al_2Cl_7^- + 3e^- \leftrightarrow Al + 7AlCl_4^-$$

Cathode:

$$C_n + AlCl_4^- \leftrightarrow C_n[AlCl_4] + e^-$$

where n is the molar ratio of carbon atom to intercalated anions in the graphite. Because stage transitions proceed continuously during cycling—yielding mixed stages and a sloping voltage profile—the GIC is written generically as $C_n[AlCl_4]$, where n changes with state of charge rather than assuming a fixed stoichiometry.[15] In addition to intercalation, reversible adsorption/desorption of $AlCl_4^-$ may also occur in micro-/meso-pores of cathode materials with large specific surface areas.[17] Consequently, the electrolyte serves as the anolyte for the carbon cathode and as the catholyte for the Al anode. Given the high theoretical capacity of the metal anode, either the cathode or the electrolyte can be a capacity-limiting component in the system.

Research on AGDIBs has mainly emerged within the past decade, with a limited number of studies making notable contributions; nevertheless, the field remains in its infancy and requires further exploration. AGDIBs have undergone notable advancements in key components such as anode, electrolyte, and cathode to improve their overall performance. Fig. 2 summarizes the key characteristics of the battery components and the associated challenges. The anode, typically made of Al,

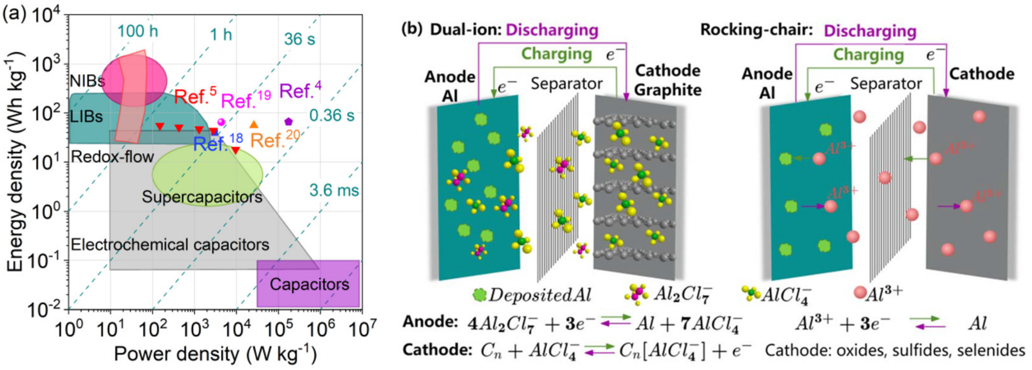

Fig. 1 (a) Ragone plot of AGDIBs reported on the literature[4,5,18–20] in comparison with lithium-ion batteries (LIBs), electrochemical capacitors, capacitors, sodium-ion batteries (NIBs), supercapacitors, and redox flow batteries. (b) Schematic charge storage mechanisms of dual-ion and rocking-chair batteries during the charge/discharge process. The different colors used to represent Al in $Al_2Cl_7^-$ and $AlCl_4^-$ are purely for visual distinction and do not reflect any actual difference in chemical identity or oxidation state.

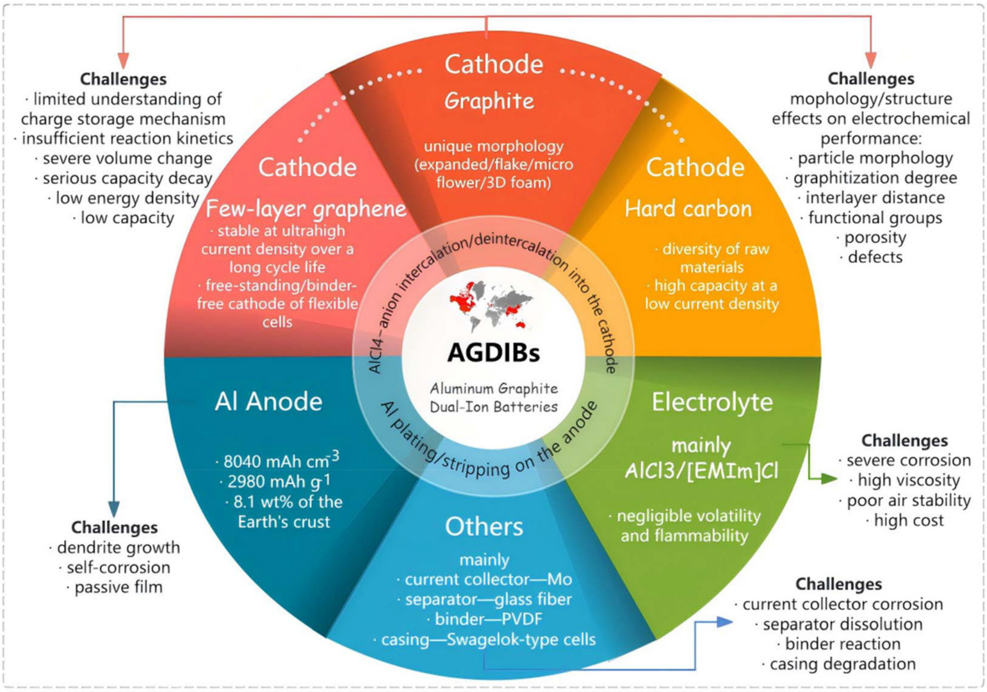

Fig. 2 Characteristics and challenges throughout the cell components of AGDIBs.

offers high abundance, excellent power density, and comparable energy density. However, it faces challenges such as corrosion, dendrite growth, and the formation of a passivation layer. In addition, the actual capacity of the battery is primarily limited by either the cathode materials or the electrolyte composition. Most cathodes in AGDIBs are made of graphite and few-layer graphene, which offer good rate performance but struggle with limited intercalation capacity. Some studies have explored hard carbon, which demonstrates high capacity but at low current densities. At this stage, there is a lack of understanding of the storage mechanism and the impact of structure and morphology on electrochemical performance hindering the further optimization of AGDIBs. Chloroaluminate-based ionic liquids, such as $AlCl_3$/[EMIm]Cl, are widely employed due to their negligible volatility, low flammability, and, most importantly, their unique electrochemical behavior. These electrolytes enable both reversible Al plating and anion intercalation, thanks to the presence of two distinct chloroaluminate species. This dual functionality has not been achieved with many other solvents, particularly those that are chloride-free. The anolyte exhibits a specific capacity ranging from 21 to 46 mAh g^{-1}, depending strongly on the $AlCl_3$: [EMIm]Cl molar ratio (ranging from 1.3 to 2.0) and the applied current density.[21] However, this electrolyte is highly corrosive to other cell components, posing challenges in selecting suitable materials for the battery. Overall, research has mainly targeted optimization of graphitic cathodes to enhance battery performance, alongside efforts to mitigate Al corrosion through anode modification or the use of less corrosive electrolytes. However, limited understanding of the Al–electrolyte interface, conflicting views on cathode intercalation mechanisms, and severe corrosion in imidazolium-based electrolytes highlight critical gaps and opportunities for further investigation. In this review, recent advances in the development of AGDIBs are summarized, with an emphasis on key findings from recent literature. From the perspective of practical application, major challenges and potential solutions related to various cell components are critically discussed. Finally, a summary and outlook are provided to guide future research on high-performance component materials and to support the advancement of practical, next-generation AGDIBs.

2. Anodes

The utilized anode in AGDIBs is generally metallic Al, in the form of foils/rods/wires according to cell configurations, to support Al plating/stripping. Kravchyk *et al.*[22] stated that starting with a bulk metallic Al anode is not a necessity. Instead, any current collector supporting the initial electroplating of Al or coated with a thin Al seed layer is sufficient. The impacts of using such current collectors on storage mechanisms need to be considered. Besides, coating is an extra step that adds complexity, cost, and time to the overall manufacturing process. Batteries using graphite anode[23,24] instead of Al, with graphite cathode and an $AlCl_3$/[EMIM]Cl electrolyte, have been presented. These two studies propose different storage mechanisms, highlighting the lack of understanding of this battery system. However, it is important to note that the system investigated is not technically an AGDIB. While using Al as anode,

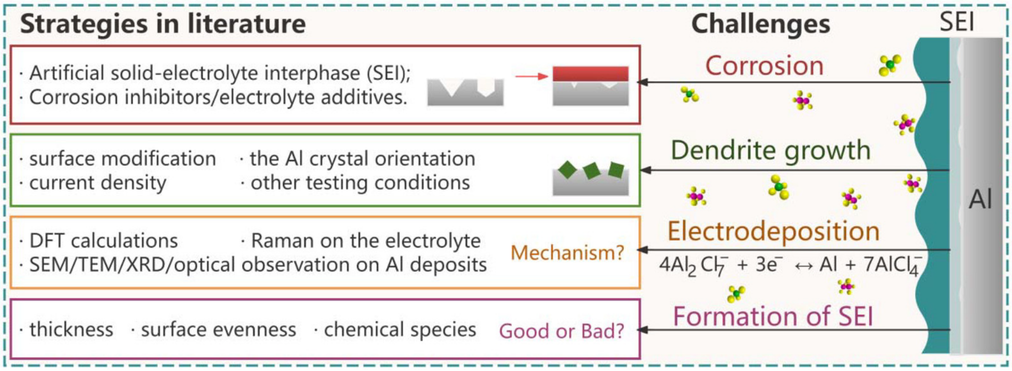

Fig. 3 Schematic of anode issues and published strategies on anode-electrolyte interface.

it presents several persistent challenges that hinder stable cycling performance (Fig. 3). These challenges include the Al anode's susceptibility to corrosion in aggressive electrolytes and the formation of dendrites with morphologies distinct from conventional tree-like structures. Besides, the underlying mechanisms governing Al electrodeposition remain complex and not fully understood. Moreover, conflicting reports exist on the impact of passivating surface films, which can either mitigate or simultaneously exacerbate corrosion and dendrite formation. Owing to the high chemical activity of Al in the electrolyte, the surface of the Al anode illustrates complicated reactions. The interface between the anode and electrolyte plays a vital role for battery performance, hence improvements related to the anode focus on the anode/electrolyte interface.

2.1 Corrosion

Corrosion of the Al anode is a big challenge in AGDIBs due to the highly corrosive electrolytes. The metal impurities and crystallographic orientation of the Al anode influence the degree of corrosion. The metallic Al anode contains impurities such as iron, silicon, and copper, where in particular iron exists even under high purity (99.999%). Iron with less negative electrode potentials can form galvanic cells with Al, causing a higher corrosion rate to Al itself. Therefore, reducing impurities, particularly iron, can help alleviate Al corrosion. On the other hand, a study by Ghadir Razaz *et al.*[25] reveals that a larger surface-area corrosion caused by up to 1 wt% iron impurity leads to an enhancement in capacity and cycle life. It implies that iron exists as an intermetallic phase, namely Al_3Fe, in Al. The evenly distributed Al_3Fe phase provides locations for the electrolyte to break down more easily, increasing the electrode area involved in the electrochemical reactions. Higher purity Al also means a higher cost. Utilizing lower purity Al allows recycled Al to be reused, thus reducing energy consumption, environmental impact, and cell cost. Trace metal ion impurities present in the electrolyte deposit on the Al anode within the battery soon after assembly,[26] which is also claimed to have caused the pitting corrosion and highly uneven Al deposits.[27] Basically, crystallographic orientation of the planes parallel to the surface can also affect the corrosion behavior of metals. In addition, Al with a (110) crystallographic orientation was found to demonstrate the strongest corrosion in NaOH and KOH solutions because of having the highest surface energy.[28] Newly formed lattice planes (111), (220), and (311) were observed in dipping experiment of pristine Al (200) in $AlCl_3$/[EMIM]Cl electrolytes.[29] However, there is no systematic study on the influence of the crystallographic orientation on the corrosion resistance of Al in AGDIBs. Thus, the effects and mechanisms of different impurities and crystallographic orientations on Al corrosion and cell performance remain still to be explored and understood. In full cell cycling, the corrosion can take place at any time once in contact with electrolytes, but the corrosion may be more significant at discharging state due to the higher $Al_2Cl_7^-$ concentration. This highlights the need for effective strategies to mitigate corrosion, which are essential for ensuring long-term cell stability and performance.

Currently, common solutions to corrosion are limited to surface modifications that create an artificial solid-electrolyte interphase (SEI). This surface layer affects not only corrosion but also Al plating/stripping. Coating an SEI layer on Al anode as an inert physical barrier allows the electrolyte to homogeneously infiltrate the surface of the Al anode, which makes the corrosion on the Al anode surface more uniform. Consequently, it generates a uniform Al plating/stripping rather than dendrite growth. Graphite was constructed on Al foil by simple blade coating method as an SEI layer.[30] After 40 h cycling at 0.1 mA cm^{-2} current density, the pristine Al shows big, corroded areas (15 μm), while no obvious corrosion can be observed on the surface of the Al anode underneath the SEI layer. However, the electrochemical performance was not outstanding, and no analysis on the possible participation of the graphite layer in the storage mechanism was provided. Corrosion inhibitors were used in electrolytes to create dense and uniform barrier SEI layers on electrodes, which not only mitigate the corrosion but also dendrite growth. An *ab initio* molecular dynamics (AIMD) simulation suggests that proper additives can preferentially form stable SEI layers.[31] Nonionic surfactant F127[32] and cetyltrimethyl-ammonium chloride (CTAC)[33] were used as corrosion inhibitors in $AlCl_3/Et_3NHCl$

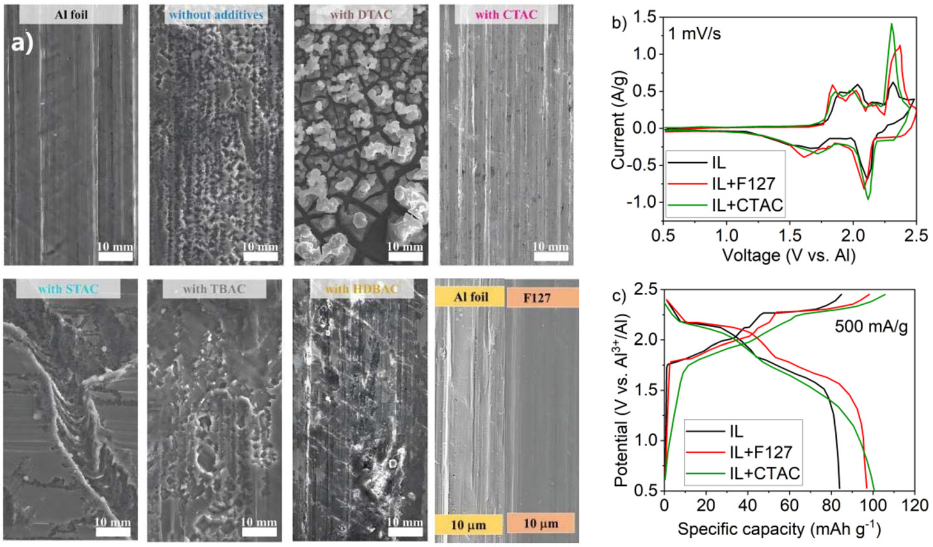

Fig. 4 (a) The SEM images of Al foil soaked in the $AlCl_3/Et_3NHCl$ (1.5 : 1) electrolyte and the ones with different additives: F127, dodecyltrimethylammonium chloride (DTAC), cetyltrimethyl-ammonium chloride (CTAC), stearyltrimethylammonium chloride (STAC), tetrabutylammonium chloride (TBAC), and benzyldimethylhexadecylammonium chloride (HDBAC). (b) CV curves and (c) charge/discharge profiles of Al//FG full batteries using electrolyte with/without F127 and CTAC additives. Adapted with permission from Elsevier.[32] Copyright 2024. Adapted with permission from John Wiley and Sons.[33] Copyright 2024.

(1.5 : 1) electrolytes, respectively. The consequent barrier layers mitigate the corrosion and effectively induce uniform Al plating/stripping on anode (Fig. 4a). The intercalation mechanism into graphite was not affected, while the cells with additives illustrate higher specific capacities at a current density of 500 mA g^{-1} (Fig. 4b and c). A pretreatment (alkali-assisted boiling water treatment) followed by an anodizing process to the Al foil was reported.[34] This pretreatment generates an artificial SEI (a hydrated oxide film) which then transforms into a denser anodic oxide film (391 nm thickness of Al_2O_3) and a flake-like outer layer ($Al_2O_3{\cdot}H_2O$). This process has been shown to enhance the corrosion resistance of the Al anode. In brief, the creation of an artificial SEI or the addition of corrosion inhibitors can effectively mitigate Al corrosion.

However, the role of the native Al_2O_3 film on Al anode remains a subject of considerable debate. Metallic Al is naturally covered with an Al_2O_3 layer owing to the high reactivity of pristine Al. While this surface oxide is intrinsically both ionically and electronically insulating, its presence has been reported to exert either protective or detrimental effects, depending on its thickness and uniformity. The native oxide layer on the Al surface can be attacked and dissolved by chloroaluminate anions ($AlCl_4^-$ and $Al_2Cl_7^-$) of the corrosive $AlCl_3$/[EMIm]Cl electrolyte, exposing a fresh Al surface directly to the electrolyte for Al dissolution and deposition reactions. This process prevents complete passivation and enables reversible Al plating/stripping; however, it simultaneously promotes progressive surface degradation. A dipping experiment of Al metal in $AlCl_3$/[EMIm]Cl electrolyte indicates severe pitting corrosion, which becomes more pronounced in more acidic compositions—*i.e.*, at higher $AlCl_3$ molar ratios—where the concentration of $Al_2Cl_7^-$ species is elevated.[29] The pitting corrosion and deposition of the newly formed Al oxide on the defective sites results in growing cracks and fragments on the Al metal surface.

Conflicting findings have been reported regarding the influence of oxide thickness. A thicker Al_2O_3 layer can better shield the Al anode from aggressive electrolytes, mitigating corrosion effects.[35,36] Yet, excessive thickening imposes kinetic limitations by hindering electron transfer and increasing the nucleation barrier for Al deposition, thereby elevating polarization, especially at high current densities.[37] In contrast, thinner oxide films (<50 nm) have been shown to suppress dendritic growth, and their removal was correlated with markedly poorer cycling stability in Al//graphite cells.[38] Electrochemical pretreatments such as electropolishing, which leave behind an ultrathin oxide layer, result in a larger electrochemically active surface area. Although such surfaces exhibit more evident localized corrosion, the corresponding full cells display enhanced capacity and cycling stability.[14,39]

Recent studies further suggest that the passivation layer is chemically more complex than a simple Al_2O_3 film. Instead, cycling generates a stratified passive film consisting of an outer inorganic/organic layer (including carbonates, chlorides, and nitrides) and an inner oxide-rich region.[40] This structural and compositional heterogeneity highlights the multifaceted role of surface passivation. While it may partially protect the Al anode against corrosive electrolytes, it can also aggravate surface degradation under certain conditions, thereby complicating interfacial processes and electrochemical performance. Current understanding of the formation, dissolution, and structural evolution of this oxide layer remains limited, and systematic studies—combining advanced structural characterization with theoretical modeling—are required to elucidate its governing mechanisms and to guide rational interface engineering strategies.

2.2 Electrodeposition and dendrite growth

Electrodeposition typically occurs only during the charging process and is expected to be uniform. However, nonuniform current density distributions during charge–discharge cycling —arising from pitting corrosion and related factors—can promote dendrite growth. The widely accepted charge storage mechanism at the anode involves cathodic deposition (plating) of aluminum during charging and anodic dissolution (stripping) during discharging. Although corrosion and dendrite growth are distinct phenomena, they are closely interrelated—localized corrosion can create surface inhomogeneities or defects that act as initiation sites for dendritic growth under electrochemical deposition conditions. Several publications have corroborated reaction $4Al_2Cl_7^- + 3e^- \leftrightarrow Al + 7AlCl_4^-$ and further elaborated on the reaction intermediates and rate limitations, offering deeper insights into the mechanisms. A kinetic study combined with density functional theory (DFT) calculations was performed to investigate the Al plating/stripping in Lewis acidic $AlCl_3$/[EMIm]Cl (2 : 1) electrolyte.[41] In this study, two primary rate-limiting steps have been proposed during Al plating. The first is a chemical step involving the sequential release of chloride ions (Cl^-) from aluminum chloride complexes, represented as $AlCl_m^- \rightarrow AlCl_{(m-1)} + Cl^-$, $m = 3, 2, 1$. The second involves an electrochemical step where Al undergoes a stepwise reduction from its trivalent (Al^{3+}) to monovalent (Al^+) oxidation state by accepting electrons, exhibited as $Al^{m+} + e^- \rightarrow Al^{(m-1)+}$, $m = 3, 2, 1$. These processes are governed by the kinetics of Al speciation and complexation in the electrolyte. Conversely, during stripping, the rate-determining mechanism involves a sequence of three single-electron transfer steps, coupled with chemical reactions that release chloride ions back into the electrolyte. The efficiency and reversibility of Al plating/stripping are highly dependent on the dynamics of Al-based complex ions, particularly $AlCl_4^-$, $Al_2Cl_7^-$, and other chloroaluminate species. The speciation and interconversion of these anions influence not only the deposition rate but also the morphology and uniformity of the Al layer. Furthermore, side reactions involving intermediate species at the Al surface, as well as the electrolyte concentration and composition, play critical roles in the evolution of the anode surface. These factors must be carefully considered when analyzing the electrochemical behavior and long-term stability of Al anodes in AGDIB systems.

Al is often considered a dendrite-free metal; however, various electrodeposition morphologies resembling dendrites have been observed and are commonly referred to as “dendrites” in the literature. Craig *et al.*[42] reported that Al's face-centered cubic crystal structure, characterized by a high coordination number of 12, promotes dense and uniform metal deposition due to its energetically favorable atomic reorganization. This behavior contrasts with metals possessing lower coordination numbers. Dendrites are expected to only form at high current densities above 100 mA cm^{-2},[13] which is significantly above the typical operational range (up to 10 mA cm^{-2})[1] in AGDIBs. Thus, a key advantage of Al is its dendrite-free behavior at moderate current densities when plated onto suitable substrates such as aluminum, tungsten, or planar vitreous carbon. Elia *et al.*[43] observed extensive pitting and irregular deposit morphology after 500 cycles but reported no evidence of protruding dendritic structures. Nevertheless, several studies have documented dendrite formation in AGDIBs, indicating that this issue remains under investigation. In general, the electrodeposition process initiates with nucleation, followed by the growth of the deposited layer. Once a crystal structure is established, further growth becomes limited by either diffusion or interfacial kinetics, depending on which process is slower. Dendrite formation is typically associated with inhomogeneous electrodeposition during repeated Al plating and stripping cycles. In AGDIBs, dendritic growth on Al foil is often attributed to uneven surface corrosion and the presence of impurities at the anode–electrolyte interface (Fig. 5). These dendritic structures are typically less electrochemically active than pristine Al, resulting in uneven current distribution and localized charge accumulation. Consequently, Al tends to deposit preferentially at regions of higher electric field intensity and reduced ion diffusion distance, promoting dendrite growth—particularly under high current densities.[1,13,42,43]

In fact, the formation of dendrites is influenced by several factors, including crystal orientation, surface roughness, current density, and so on. Compared to the dense, continuous, and well-adherent Al electrodeposition shown in Fig. 6a, various other morphologies have been reported. Flake-shaped deposits, which cover the Al substrate homogeneously, were

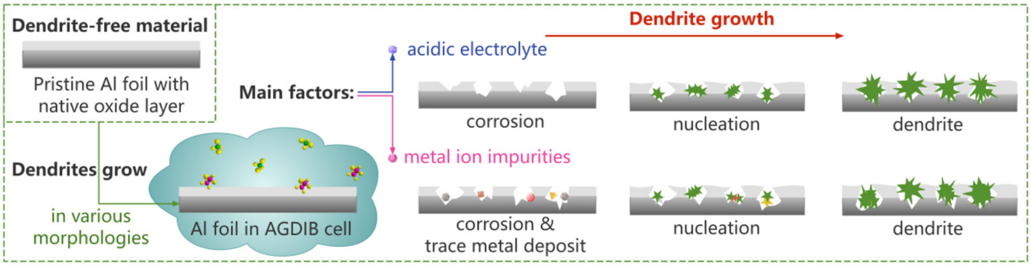

Fig. 5 Schematic illustration of dendrite formation on the Al anode, despite its intended role as a dendrite-free material.

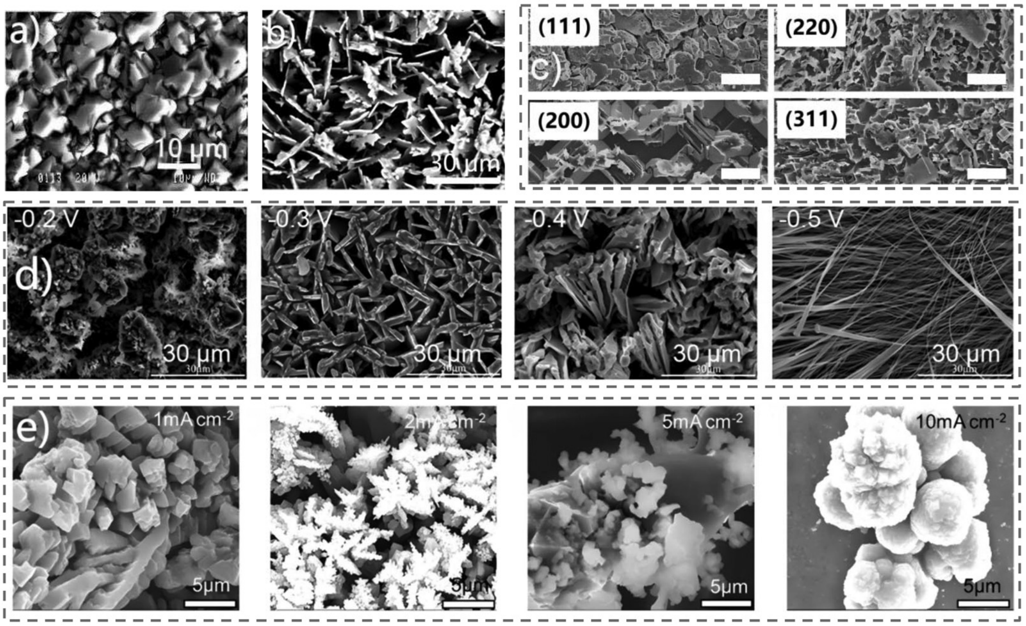

Fig. 6 SEM images of Al surface with electrodeposited Al: (a) faceted structure after 20 min at 60 °C and −0.30 V. Reproduced with permission from Elsevier.[13] Copyright 2006. (b) Homogeneous coverage with flake-shaped deposits. Reproduced with permission from Elsevier.[44] Copyright 2018. (c) Varying morphologies due to the primary crystal orientations after 50 cycles. Scale bar: 10 μm. Reproduced with permission from Springer Nature.[45] Copyright 2024. (d) SEM image of the electrodeposited Al on Cu substrate at 313 K for 1 h under potential of −0.2 V to −0.5 V, using a three-electrode system with $AlCl_3/Et_3NHCl$ (1.7 : 1) electrolyte. Reproduced with permission from Springer Nature.[12] Copyright 2024. (e) SEM images of Al surface with electrodeposited Al with increasing current density between 1 and 10 mA cm^{-2} using a symmetric battery with $AlCl_3$/[EMIm]Cl (1.3 : 1) electrolyte. Reproduced with permission from IOP Publishing Limited.[37] Copyright 2020.

observed in an $AlCl_3$: [BMIm]Cl (2 : 1) electrolyte (Fig. 6b).[44] As shown in Fig. 6b, these deposits are planar, thin, and large, vertically oriented to form walls with an average width of 20 μm and a thickness of less than 3 μm. Wang *et al.*[45] reported that Al tends to form (111) crystal planes during electrodeposition in $AlCl_3/Et_3NHCl$ (1.5 : 1) electrolyte. The charge transfer resistance of (111) Al electrodes is significantly lower than (200) Al, (220) Al, and (311) anodes, indicating its faster Al plating/stripping reaction kinetics. As a result, choosing Al with preferred (111) crystal plane as anode could obtain high lattice matching between the substrate and deposited metal, allowing uniform deposition of the Al (111) plane on the Al surface, as shown in Fig. 6c. On the other side, it found that the Al deposition displays a preferential crystallographic orientation along the (200) plane in both $AlCl_3/Et_3NHCl$[12] and $AlCl_3$/[EMIm]Cl[46] electrolytes; however, no in-depth explanation to why this is the case was presented. Besides, deposition potential was also found to affect the deposits morphology (Fig. 6d).[12] At a deposition potential of −0.3 V, the Al deposition layer appears relatively uniform and dense. However, when the potential is further decreased to −0.5 V, the layer shows the formation of nanowire structures with an approximate diameter of 367 nm. Additionally, the thickness of the deposition layer increases significantly, from 40.47 μm to 127.3 μm, accompanied by a rise in surface roughness. She *et al.*[37] found that dendrite growth involves a series of complex processes, including nucleation, growth, and stripping. The density of dendrites increased with increasing current densities between 1 and 10 mA cm^{-2}, and the corresponding morphological evolution varied from needle-like to spherical shape (Fig. 6e). The dendrites formed during the initial cycles dissolve over time due to contact with a large excess of acidic electrolyte.[46] Overall, dendrite formation has been reported in the literature, and it can be mitigated by controlling factors such as the crystallographic orientation of the anode, surface morphology, current density, and other experimental conditions.

Various strategies have been proposed to suppress dendrite formation on aluminum anodes, with most efforts centering on surface modification techniques, particularly the introduction of an Al_2O_3 layer to regulate deposition behavior. The strong oxygen-mediated bonding between Al deposits and the substrate has been reported to facilitate uniform planar growth along the interface.[47] For instance, immersion in boiling water followed by phosphoric acid treatment yields a dense ∼100 nm aluminum phosphate layer that allows Al deposits to form without significant dendrite growth.[48] Interestingly, some studies reported that a uniform Al_2O_3 layer on the surface could efficiently restrict the growth of crystalline Al dendrites and thus improve the cycling stability of the Al anode.[38] Other approaches combine surface modification with substrate design, such as fabricating a micro-porous Al substrate with a partial Al_2O_3 coverage and leaving oxide-free regions to direct localized deposition.[1,49] However, the long-term viability of these strategies remains questionable. In

Table 1 Reported modifications on Al electrodes in dual-ion batteries with Al anodes and graphite cathodes over the years

			Long-term cycling				
Anode|cathode	Electrolyte	Specific capacity (mAh g^{-1})/current density (mA g^{-1})	Specific capacity (mAh g^{-1})	Current density (mA g^{-1})	Capacity retention	Cycle number	Year [Ref.]
(111) Al[a]|three-dimensional graphite	$AlCl_3/Et_3NHCl$ 1.5 : 1	102/1000	80	5000	80.0%	25 000	2024 [45]
BPA@Al |three-dimensional graphite	$AlCl_3/Et_3NHCl$ 1.5 : 1	112/500	96.7	5000	97.8%	20 000	2024 [48]
2P-Al_2O_3 /Al|graphite	$AlCl_3/Et_3NHCl$ 1.5 : 1	80/20	78.8	100	95%	1000	2023 [49]
P-Al_2O_3 /Al|flake graphite	$AlCl_3/Et_3NHCl$ 1.5 : 1	79.2/1C rate	82.4	2C rate	94.3%	500	2023 [1]
Graphite coated Al|flake graphite	$AlCl_3$/[EMIm]Cl 1.3 : 1	—	98	100	97%	740	2023 [30]
Electropolished Al|graphite	$AlCl_3$/[EMIm]Cl 1.3 : 1	90/1000	53	5000	72%	10 000	2022 [14]
3D Al foam|graphite	1 M $LiPF_6$ in EMC/VC*	—	105	100	96%	600	2020 [50]
nAl@C |graphite	4 M $LiPF_6$ in EMC/VC	91/200	88	1500	94.6%	1000	2018 [51]
CHA-Al |expanded graphite	4 M $LiPF_6$ in EMC	98/5C rate	100	2C rate	99%	1500	2017 [52]
3D pAl/C |graphite	4 M $LiPF_6$ in EMC/VC	85/20C rate	93	2C rate	89.4%	1000	2016 [53]

[a] (111) Al: Al anode with (111) preferred crystal plane. BPA@Al: Al anode prepared by a simple boiling water treatment followed by phosphoric acid immersion. 2P-Al_2O_3/Al: A microporous Al coated with aluminum oxide, with the bottom intentionally left uncoated. P-Al_2O_3/Al: A microporous Al with the upper surface coated with an aluminum oxide layer. EMC/VC: ethyl methyl carbonate with an addition of 5 wt% vinylene carbonate. nAl@C: core/shell aluminum@carbon nanospheres. CHA-Al: carbon-coated hollow aluminum nanospheres on Al foil. 3D pAl/C: 3D porous Al coated by carbon layer.

highly acidic electrolytes, the Al_2O_3 film readily dissolves and cannot function as a persistent barrier, while its pitting corrosion often introduces surface inhomogeneities that accelerate dendrite growth. Consequently, the role of Al_2O_3 layers in dendrite suppression remains controversial, warranting further systematic investigation.

Table 1 summarizes the reported modifications of Al anodes in dual-ion batteries with graphite cathodes. Early studies mainly investigated Al volume changes in $LiPF_6$/EMC-based Al//graphite systems, which are essentially lithium-ion batteries.[50–53] In contrast, research on AGDIBs—typically employing $AlCl_3/Et_3NHCl$ or $AlCl_3$/[EMIm]Cl electrolytes—has focused primarily on surface treatments, protective coatings, and composite designs to suppress corrosion and promote uniform electrodeposition. However, only a few studies have extended these investigations to demonstrate meaningful improvements in full-cell cycling performance. More recent reports suggest that surface engineering strategies such as electropolishing, controlled oxide layer formation, and carbon-based coatings have enabled stable operation over extended lifetimes, with reports of up to 25 000 cycles. Despite these advances, most work has emphasized interfacial stabilization rather than practical battery metrics, and fundamental issues such as the volume change of Al electrodes in AGDIBs remain unexplored, representing a key knowledge gap in the field.

Beyond interfacial stability and electrochemical performance, the sustainability dimension of AGDIBs—particularly the environmental and economic implications of aluminum extraction and recycling—remains insufficiently addressed. Despite aluminum's abundance, its extraction is highly unsustainable due to energy-intensive smelting and associated environmental damage. In 2021, global primary Al smelting capacity reached 81 million tons per year, generating total emissions of 651 million metric tons of CO_2 equivalent, with 82% of these emissions stemming from electricity use and 18% from the smelting process itself.[54] The process also releases other pollutants, including perfluorocarbons, and causes land degradation and water pollution, particularly from bauxite mining. Efforts to reduce these impacts include increasing Al recycling, which cuts CO_2 emissions by 95%, and adopting cleaner energy in production.[55] Though both Al mining and recycling have environmental impacts, recycling is undoubtedly more sustainable than primary production. Ideally, efforts should focus on reducing the demand for primary Al and improving the efficiency of recycling systems. While Al-based batteries may contribute to increased overall Al demand, they offer notable advantages over lithium-ion batteries, such as greater supply security, material abundance, and recyclability. At present, however, high-purity Al foils are required to prevent side reactions caused by trace impurities, significantly increasing production costs. As of 2024, the prices of high-purity aluminum were exceptionally high: 4N (99.99%) at €261.95 per kg, 5N (99.999%) at €475.95 per kg, and 6N (99.9999%) at €950.95 per kg.[56] Maximizing the use of recycled Al in battery manufacturing will therefore be essential to balance performance with sustainability.

In conclusion, the Al anode in AGDIBs presents several key advantages, including low cost, high volumetric capacity, excellent recyclability, and the potential for dendrite-free plating/stripping under moderate current densities. Nonetheless, key challenges remain:

- Corrosion in aggressive electrolytes undermines interfacial stability and long-term performance.
- Dendrite formation, though less severe than in Li systems, arises from impurities, current-density inhomogeneities, and complex multi-step plating/stripping kinetics.
- Al_2O_3 surface films show inconsistent effects, leaving interfacial reactions poorly understood.

Future progress will depend on elucidating interfacial mechanisms, optimizing electrolytes, and developing deposition-regulation strategies to ensure durable anode operation.

3. Cathodes

To date, cathode materials for AGDIBs are dominated by graphite. Graphite is considered one of the most promising cathode candidates due to its high electrical conductivity, chemical stability, and, most importantly, its layered graphene structure enabling reversible anion intercalation and deintercalation during cycling. Despite these advantages, graphite cathodes face several challenges, including relatively low reversible capacity, sluggish ion diffusion kinetics, and structural expansion during cycling.[57] Moreover, the underlying storage mechanisms are not yet fully understood. Over the past decade, about a hundred studies have focused on graphitic carbon cathodes for AGDIBs, leading to significant progress. Graphite accounts for over 66% of published AGDIBs cathode materials, followed by approximately 21% few-layer graphene and 13% hard carbon.

3.1 Graphite

Graphite materials with different structural characteristics, flakes, expanded layers, and 3D porous structures have been studied extensively in AGDIBs over the past decade. Inexpensive natural graphite (NG) is the most used cathode material by far. An Al//NG full cell[5] demonstrated a high capacity of 110 mAh g^{-1} at a current density of 20 A g^{-1}, an ultra-fast charge/discharge time of just 9 seconds, and remarkable cycling stability—retaining 70% capacity after 500 000 cycles. Compared to pyrolytic graphite (PG) and synthetic graphite (SG), NG showed a larger cyclic voltammetry (CV) area in the 1.80–2.25 V range, indicating easier dilute-stage intercalation.[58] CV measurements with NG cathodes also revealed five sharp, well-defined reversible peaks (Fig. 9a),[59] suggesting a uniform multistage intercalation process. A free-standing NG film was attached to Ni bar current collectors using conductive carbon tape, which delivered a significantly higher specific capacity than PG free-standing cathode due to better structural reversibility.[60] *In situ* Raman spectroscopy and *ex situ* XRD confirmed NG's highly reversible structural changes during charge/discharge. In contrast, the (002) XRD peak of PG did not fully return to its original state after discharge, indicating residual strain and structural disorder in the PG material. Overall, the flaky morphology and well-ordered atomic structure of NG facilitate efficient $AlCl_4^-$ intercalation and highly reversible structural changes.

In addition to intercalation, adsorption within pores may also contribute to a higher capacity. Kish graphite (KG), a synthetic flake-shaped graphite, is available on a large scale as a byproduct of steel manufacturing. Besides its flake structure, KG possesses macro-structural defects such as holes and cracks. As cathode, the intercalation of $AlCl_4^-$ ions occurs with a significant interlayer space expansion by up to 8.85 Å or 12.1 Å at intercalation stage 4 or 3 GICs, respectively.[19] Large-sized kish graphite flakes with high structural perfection (Raman spectra I_D/I_G = 0.05) showed exceptional rate capability, yielding a high power density of 4363 W kg^{-1}. High-quality Kish expanded graphite (KEG) cathode materials were synthesized from KG through a simple and rapid expansion process.[17] As shown in Fig. 7a, the CV curves of KEG demonstrate excellent reversibility and stability in anion storage, which involves both diffusion-controlled intercalation and a significant contribution from adsorption-controlled processes. At higher current densities, $AlCl_4^-$ anion storage becomes increasingly dominated by surface adsorption. Compared to unexpanded KG (Fig. 7a),[61] the increased proportion of capacitive, adsorption-controlled behavior in KEG can be attributed to its fluffy micro-nano interlayer pore structure, which is formed by the cross-linking of single or few graphene layers. This porous architecture enhances anion accessibility and adsorption, leading to a notable improvement in specific capacity—from approximately 110 mAh g^{-1} to 140 mAh g^{-1} at 50 mA g^{-1} (Fig. 7b). Thus, the introduction of hierarchical pores effectively promotes additional adsorption sites, thereby boosting the overall storage capacity.

By constructing a highly porous three-dimensional graphitic foam that allows fast ion diffusion/intercalation can facilitate more rapid battery operation. A pioneering work using a 3D graphitic foam cathode, deposited on a nickel foam template by chemical vapor deposition, was published by Lin *et al.*[18] in 2015. The Al//graphitic-foam pouch cell demonstrated a charging capability at a current density up to 5 A g^{-1}, about 75 times higher than the Al//pyrolytic graphite cell, while maintaining a similar voltage profile and discharge capacity (~60 mAh g^{-1}). The cell sustained over 7500 cycles without capacity loss and achieved energy and power densities of 40 Wh kg^{-1} and 3000 W kg^{-1}, respectively. They further prepared a 3D graphitic foam containing vertically aligned few-layered graphene sheets as cathode materials.[62] This shows that a low density of defects and oxygen groups can increase accessible spaces for $AlCl_4^-$ intercalation, leading to a higher capacity and a lower cutoff charge voltage.

It was found that only highly graphitic materials can intercalate $AlCl_4^-$ anions, whilst the amorphous part of the carbon hinders the accessibility of $AlCl_4^-$.[63] In Fig. 7b, acetylene black (AB) shows only a slope without a plateau, whereas natural graphite flakes (NGF) and kish graphite flakes (KGF) display typical graphite intercalation storage curves, characterized by both slope and plateau. Thus, to achieve high-quality graphite materials, not only abundant layers, porous morphologies (to facilitate diffusion) and adjustable interlayer spacing (for reversible anion intercalation and deintercalation), but also a high degree of graphitization (for enhanced conductivity) is required. Through a catalyst-free electrochemical graphitization, a flake graphite feature with high graphitization degree and crystallinity is easy to obtain from certain amorphous carbons.[64,65] The graphitization was carried out in molten $CaCl_2$ showing advantages of high-efficiency, low-temperature, environmentally friendliness and catalyst-free features. By this method, a nanosheet-bricked porous graphite (CB-G) was derived from carbon black (CB), presenting high crystallinity with an I_D/I_G of 0.11 and 37–38 layers of graphitic lattice planes.[66] Even at a high current density of 100 A g^{-1}, the specific capacity of CB-G maintains 90 mAh g^{-1}. In Fig. 7c, the

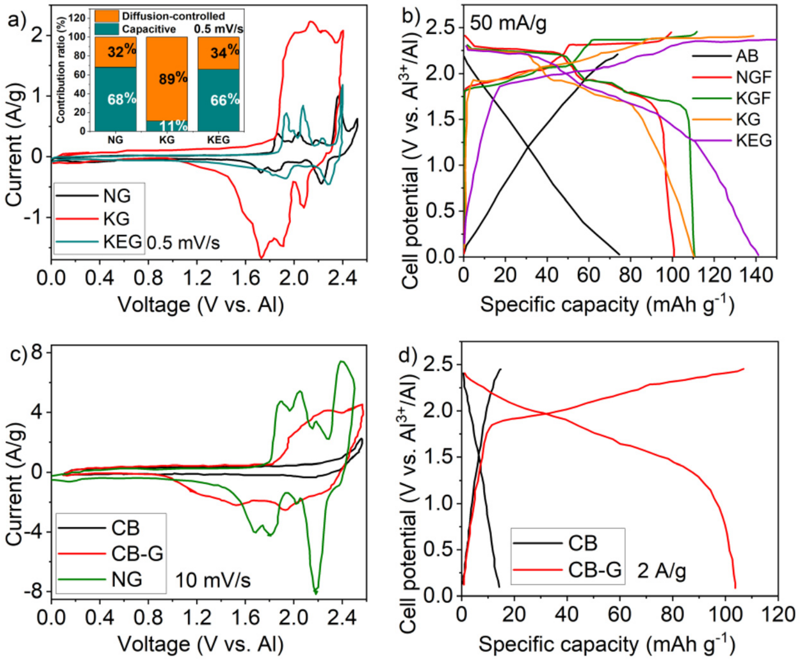

Fig. 7 (a) CV curves of cells with natural graphite (NG),[59] Kish graphite (KG)[61] and kish-based expanded graphite (KEG)[17] cathode and $AlCl_3$/[EMIM]Cl (1.3 : 1) electrolyte, at a scan rate of 0.5 mV s^{-1}. Insert is the contribution ratio of these three graphite cathodes. (b) Charging and discharging profiles of cells with various graphitic materials and $AlCl_3$/[EMIM]Cl (1.3 : 1) electrolyte at 50 mA g^{-1}. These graphite materials are KG[61] and KEG,[17] and kish graphite flakes (KGF, 2 mm), natural large graphite flakes (NGF, 1 mm) and acetylene black (AB, 26 μm).[19] (c) CV curves at a scan rate of 10 mV s^{-1} and (d) charging/discharging profiles at a current density of 2 A g^{-1} of cells with NG[59] (only used in CV), CB (XC-72) and CB-G (carbon black-derived nanosheet-bricked porous graphite, NSPG-120)[66] cathode and $AlCl_3$/[EMIM]Cl (1.3 : 1) electrolyte. Adapted with permission from Elsivier.[17] Copyright 2024. Adapted with permission from author.[19] Copyright 2017. Adapted with permission from Springer Nature.[59] Copyright 2024. Adapted with permission from Elsivier.[61] Copyright 2023. Adapted with permission from author.[66] Copyright 2018.

CV curve of CB shows no distinct peaks, whereas CB-G, although not as pronounced as NG, exhibits oxidation and reduction peaks. The cell charge/discharge profile of CB and CB-G (Fig. 7d) illustrates intercalation capacity only in CB-G, which is reflected in the plateau. This study suggests that $AlCl_4^-$ anions are unable to intercalate into amorphous carbon but become detectable as the degree of graphitization increases. Simply increasing the carbonization temperature (*e.g.* 3000 °C (ref. 67)) could also achieve a significant improvement in rate capability.

Overall, graphite cathodes with a high degree of graphitization deliver superior capacity and rate performance in AGDIBs. From a sustainability perspective, liquid-phase ultrasonic exfoliation has been employed to recycle graphite for use as cathodes, where the resulting foam-like morphology with open structures and intrinsic defects facilitates efficient $AlCl_4^-$ intercalation/deintercalation.[59] Furthermore, spent graphitic cathodes can be regenerated through simple electrolysis,[68] underscoring the recyclability and environmental friendliness of graphite-based cathode materials for AGDIBs.

3.2 Few-layer graphene

Few-layer graphene shows outstanding performance as free-standing/binder-free cathode for flexible AGDIBs owing to its remarkable mechanical properties (accommodating the volume change during cycling) and ultrahigh charge carrier mobility (excellent electron transportation). Few-layer graphene has been used in various forms as the cathode in AGDIBs. A few-layer graphene material was convoluted into hollow carbon nanoscrolls with frizzy architectures.[69] It has similar shape as multi-walled carbon nanotubes (MWCNTs), but the performance is far beyond the reported MWCNTs cathode.[70] These nanoscrolls illustrated outstanding ability to accommodate a large volume expansion during charge/discharge and a stable cycling performance at −25 °C and 80 °C. In addition, a hybrid composite cathode was synthesized by coating few-layer graphene and MWCNTs on PG.[71] In this composite, few-layer graphene acts as a host for anion intercalation, while the carbon nanotubes prevent few-layer graphene from restacking, buffering the issue of volume change. It exhibited a 60% capacity enhancement and 3-fold improvement in overall ion diffusivity over PG. These findings leave room for future innovations or improvements in graphitic carbon cathode technology.

Though edge-few/rich few-layer graphene or graphite, made from a low temperature (600 °C) process,[72] plasma-etching,[73] and N-doping,[74–76] have been studied. The presence of structural defects in the graphene layer can deteriorate the charge/discharge performance of the cells by either decreasing the electrical connectivity or hindering $AlCl_4^-$ intercalation. As

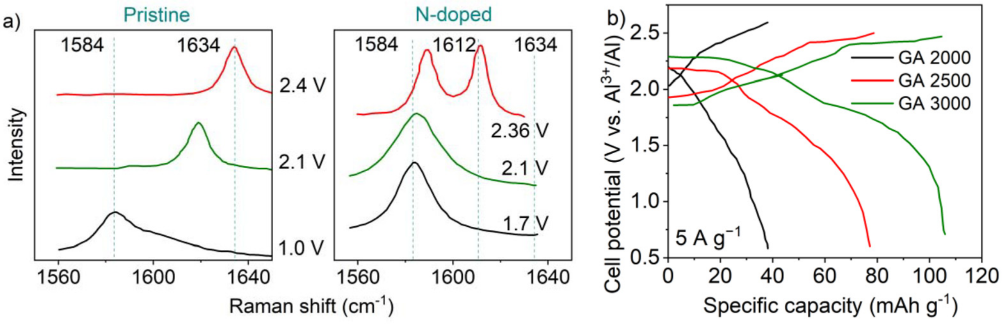

Fig. 8 (a) Part of the *in situ* Raman spectra of the pristine and N-doped few-layer graphene cathode during charge. Adapted with permission from Elsevier.[75] Copyright 2019. (b) Charge and discharge profiles at a current density of 5 A g^{-1} of the cells with few-layer graphene aerogel (GA) cathodes which were carbonized under 2000 °C, 2500 °C and 3000 °C, respectively. The I_D/I_G values of the GA samples are 0.039 (GA 2000), 0.01 (GA 2500) and approximately 0 (GA 3000). Adapted with permission from John Wiley and Sons.[77] Copyright 2017.

seen in the Raman spectra (Fig. 8a), after N-doping, the few-layer graphene cathode failed to charge properly due to poor intercalation, as evidenced by the peaks remaining in the middle stage and not fully shifting to 1634 cm^{-1}, as observed in pristine few-layer graphene. The charging process could not be completed, as the cell failed before reaching the maximum voltage. To take the most advantage of the excellent properties of graphene, a defect-free graphene sheet as large as possible is suggested for better electrochemical performance. Chen *et al.* prepared a defect-free few-layer graphene cathode with slightly stacked few-layer graphene sheets (4–10 layers) and an I_D/I_G value of almost 0 (GA 3000, Fig. 8b).[77] The achievable specific capacity increases significantly with a higher graphitization degree. By changing the charging cutoff voltage, they found that structure decomposition (defects converted from the original sp^2 carbon at a destructive charging cutoff voltage) caused the decline of cathodic capacity. They also prepared a defect-free graphene micro flower (I_D/I_G 0.0276) presenting a flower-like corrugated and fluffy morphology with numerous nanosized channels.[78] It delivered a stable capacity of 100 mAh g^{-1} over 1000 cycles at both current densities of 10 and 20 A g^{-1}. Later, a concept of "trihigh tricontinuous (3H3C)" was proposed to prepare graphite cathode.[4] It requires an ideal cathode to have high quality, orientation, and channeling (3H) for local structures and a continuous electron-conducting matrix, ion-diffusion highway, and electro active mass (3C) for the electrode. The 3H3C cathode exhibited remarkable flexibility and impressive electronic conductivity (270 000 S m^{-1}). Its vertical infiltration fissures, horizontal micrometer-sized gasbags, and nano-sized intervals collectively form interconnected 3D infiltration channels. These features contribute to a specific capacity of 111 mAh g^{-1} at 100 A g^{-1} over an impressive 250 000 cycles, maintaining a stable average discharge voltage and exhibiting low hysteresis across current densities ranging from 10 to 200 A g^{-1}. The full cell exhibits stable performances at a wide temperature range (0 to 120 °C). In short, the structural integrity and electrical connectivity of a few-layer graphene cathode must be maintained. Chemical defects, such as heteroatom-dopants, lead to poor performance.

3.3 Hard carbon

Known as non-graphitizing carbon, hard carbon has been explored in AGDIBs due to its diversity of raw materials, in particular biomass materials. The use of abundant, renewable biomass not only offers cost-effective and environmentally benign feedstocks but also aligns with circular economy principles. Moreover, the inherent structural features of hard carbon—such as hierarchical porosity, tunable interlayer spacing, and defect sites—can be tailored to facilitate ion storage while leveraging sustainable materials. However, these materials typically exhibit an extremely low degree of graphitization, which correlates with poor electrochemical performance. For instance, we found that glucose-derived and lignin-derived hard carbon materials deliver negligible capacities (<10 mAh g^{-1}) in $AlCl_3$/[EMIm]Cl (1.5 : 1) electrolyte when tested in coin cells at 500 mA g^{-1}. Interestingly, from the following literature, heteroatom doping has been found to unexpectedly enhance the electrochemical performance in AGDIBs, leading to significantly improved capacities. After N-doping, the electrical conductivity of the hard carbon xerogel (CX) decreased from 83 S m^{-1} to 62 S m^{-1} in the N-doped hard carbon xerogel (N-CX).[79] N-CX delivers a remarkably high specific capacity of over 400 mAh g^{-1} at 100 mA g^{-1}, whereas undoped CX exhibits only 10 mAh g^{-1} (Fig. 9a). Additionally, the CV curve of N-CX does not show distinct intercalation stages, unlike those seen in graphite materials. When the current density goes up to 500 mA g^{-1}, the specific capacity of N-XC experienced a quick decay to around 60 mAh g^{-1}. This suggests that the charge storage mechanism in these materials may differ fundamentally from graphite cathode.

Furthermore, an N-doped hard carbon (NC) cathode, generated from pomegranate peel (carbon base) and melamine (N source), delivered a high capacity of 323 mAh g^{-1} at 500 mA g^{-1} at the 1st cycle and 149 mAh g^{-1} after 200 cycles.[80] The charge/discharge profiles of NC exhibit plateau-like regions (Fig. 9b), suggesting possible intercalation processes. This observation is supported by the CV curve, which reveals subtle but discernible intercalation-stage characteristics. Interestingly,

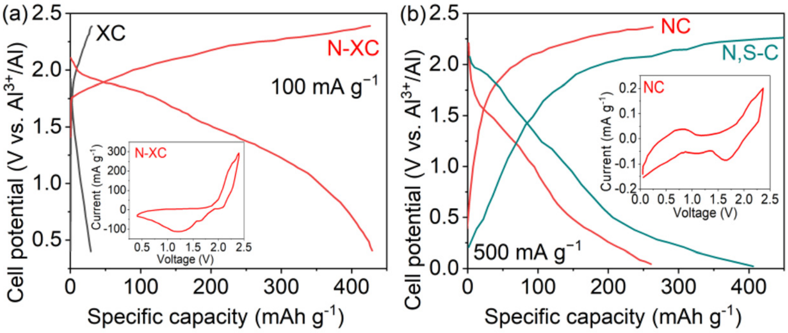

Fig. 9 (a) Charge/discharge profiles of carbon xerogel (CX) and N-CX in the 10th cycle at 100 mA g^{-1} were measured in an $AlCl_3$/[EMIm]Cl (1.5 : 1) electrolyte using a Swagelok cell; insert: CV of N-CX at a scan rate of 1 mV s^{-1} reveals redox behavior without distinct intercalation stages. Adapted with permission from Wiley.[79] Copyright 2024. (b) Charge/discharge profiles of cells with N-doped carbon (NC) at the 10th cycle at a current density of 500 mA g^{-1} in $AlCl_3$/[EMIm]Cl (1.3 : 1) electrolyte using a Swagelok cell; insert: CV at 1 mV s^{-1}. Adapted with permission from Royal Society of Chemistry.[80] Copyright 2024. Charge/discharge profiles of cells employing N,S-doped carbon (N,S–C) cathode in the 100th cycle at a current density of 500 mA g^{-1} in $AlCl_3$/[EMIm]Cl electrolyte using a Swagelok cell. Adapted from Li, J. *et al.*, *Energy Environ. Mater.*[81] Licensed under CC BY 3.0. ©2018 Wiley.

during the discharge process, $AlCl_4^-$ forms a bond with the pyridine nitrogen at the edge, and during the charging process, $AlCl_4^-$ leaves, and Cl^- forms a bond with the pyridine nitrogen at the time. This is also supported by similar results for N-XC,[79] where a strong interaction between pyridinic/graphitic nitrogen and $AlCl_4^-$ was observed. A study on AGDIBs with C_3N_4-derived layered N,S-doped carbon (N,S–C) cathode demonstrates that dual heteroatom doping significantly enhances electrochemical performance. DFT calculations reveal that N,S-co-doping reduces both the $AlCl_4^-$ adsorption energy and the work function value of the carbon matrix, thereby facilitating the reactions with $AlCl_4^-$ species at the electrode/electrolyte interface.[81] Consequently, the cell exhibited a very high capacity of 410 mAh g^{-1} at a current density of 500 mA g^{-1} and maintained 329 mAh g^{-1} after 500 cycles. The charge/discharge profiles for the cells employing NC and N,S–C cathodes exhibit similar shapes, indicating a comparable intercalation/adsorption mechanism. But the capacitive contribution of N,S–C at a sweep rate of 1 mV s^{-1} is 56.7%, which is much lower than 96% of NC.

Overall, undoped hard carbon shows poor electrochemical performance in AGDIBs. However, certain doped hard carbon materials exhibit unexpectedly high capacities—surpassing those of graphite and few-layer graphene—though only at lower current densities. This improvement is primarily attributed to the lower adsorption energy introduced by heteroatom doping, which enhances anion storage. Additionally, the large surface area and high porosity of the doped hard carbon may contribute by promoting efficient electrolyte absorption and facilitating faster anion transport.[82] Nonetheless, these factors alone cannot fully explain the significant capacity increase, suggesting that the energy storage mechanism of hard carbon is fundamentally different from that of graphite. However, the exact mechanism has not yet been clearly elucidated in current studies and remains to be further explored.

3.4 Intercalation mechanism study

In terms of the storage mechanism, three different types of compounds have been proposed: surface, substitutional, and intercalation compounds.[83] Among these, intercalation compounds—especially those involving graphite materials—have been the subject of extensive research. However, the reported levels of intercalation differ significantly across various studies. In 2013, one of the earliest studies on AGDIBs reported a system composed of an Al anode, fluorinated natural graphite cathode, and $AlCl_3$/imidazolium ([bim][Br]) ionic liquid electrolyte, suggesting the reversible intercalation of Al^{3+} into the graphite electrode, although no direct evidence was provided.[84] Subsequently, Jiao and co-workers[23,85] proposed a similar ‘rocking-chair’ mechanism involving both Al^{3+} and $[Al_aCl_b]^-$ in the charge/discharge process. However, their work only confirmed Al deposition at the anode, which does not sufficiently verify the active participation of Al^{3+}. Due to its high reactivity, Al^{3+} readily interacts with electrolytes and poses challenges for intercalation into typical cathode materials such as graphite. Notably, Lin *et al.*[18] refuted the intercalation of Al^{3+} and instead demonstrated that $AlCl_4^-$ undergoes reversible intercalation into graphite, while $Al_2Cl_7^-$ participates in Al electrodeposition at the anode—a mechanism that has since been widely accepted in the field. $AlCl_4^-$ offers more favorable electrochemical properties, including easier intercalation, better stability, and improved ionic mobility compared to Al^{3+}, addressing several challenges faced by conventional aluminum-ion batteries. However, the use of $AlCl_4^-$ as the charge carrier results in a reduced achievable cell capacity due to its larger molecular weight and lower charge per ion. During the first charge/discharge cycle, a portion of $AlCl_4^-$ anions typically becomes irreversibly trapped within the graphite structure, resulting in a slight initial capacity loss.[43,86] With continued cycling, the graphite undergoes structural reorganization, allowing more $AlCl_4^-$ anions to intercalate between the layers, which contributes to improved cell performance over time.[17]

Accordingly, the electrochemical performance of AGDIBs is highly dependent on the reversible $AlCl_4^-$ intercalation/deintercalation in cathode materials. *Ex*/*In situ* and *operando* characterizations such as Raman spectroscopy, X-ray diffraction, solid-state NMR spectroscopy, combined with theoretical modeling (*e.g.* density functional theory (DFT) and classical molecular dynamics (MD) simulations) have been applied to investigate $AlCl_4^-$ intercalation.[87–90] The interlayer space of graphite (0.335 nm) appears relatively narrow for the large ionic radius of $AlCl_4^-$ (5.28 Å). However, due to its highly tunable interlayer spacing, graphite can accommodate $AlCl_4^-$ anions, forming graphite intercalation compounds (GICs) through a unique staging mechanism that depends on the applied potential. GICs can be characterized by changes in *d*-spacing, which refers to the interplanar distance or gallery height between graphene layers. The intercalation stage index is defined as the number of graphene layers separating two adjacent intercalated layers[91,92] (Fig. 10). In the initial stage, anion intercalation progresses through highly ordered, coordinated phases as more anions are inserted into the graphite layers. Once fully charged, with the stage reaching lower numbers, the degree of order is significantly higher, suggesting that the intercalated species likely rearranged themselves further. Notably, one stage does not completely disappear before the next one begins to form.

Angell *et al.*[93] studied the intercalation stage through *in situ* Raman spectra. Fig. 11a shows part of the Raman spectra. From the very beginning of the charging process, between 1.71 and 1.94 V, the G band of pristine graphite (1584 cm^{-1}) split by 20 cm^{-1}. This splitting arises from the rearrangement of positive charges—*i.e.*, holes formed due to electron withdrawal from the graphite layers during intercalation. These holes alter the electronic environment within the graphite, leading to vibrational changes. As a result, the original band became two different E_{2g} peaks, inner (i) and outer (b). The intercalation stage (n > 2) was then calculated based on the ratio of the intensities of these two peaks on following equation:

$$\frac{I_i}{I_b} = \frac{\sigma_i}{\sigma_b}\frac{(n-2)}{2}$$

where σ_i/σ_b represents the ratio of Raman scattering cross-sections, which was assumed to be unity (16). This initial splitting was then calculated as the formation of a dilute stage of 4–5 GIC. When the cell is charged from 2.097 V to 2.3 V, only one high-intensity peak at 1632 cm^{-1} remained. They defined it as the formation of a stage 2 GIC, which, however, is unreachable according to the following XRD findings. Pan *et al.*[91] studied this stage mechanism through *in situ*/*operando* electrochemical and synchrotron X-ray diffraction experiments combined with theoretical modeling. Their calculations revealed that the gallery height of the anion intercalation layer in graphite is approximately 9.49–9.54 Å. At room temperature, a stage 4 GIC is observed at the fully charged state. However, when the temp-

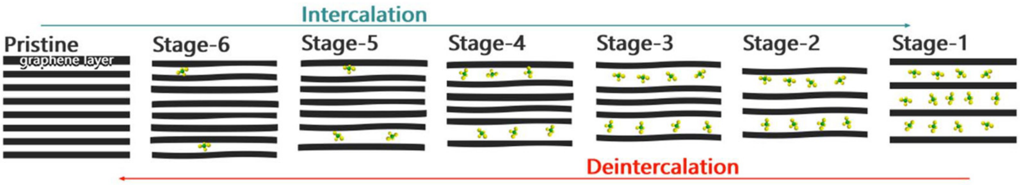

Fig. 10 Schematic image of the intercalation stage index showing the number of graphene sheets between two adjacent intercalated layers.

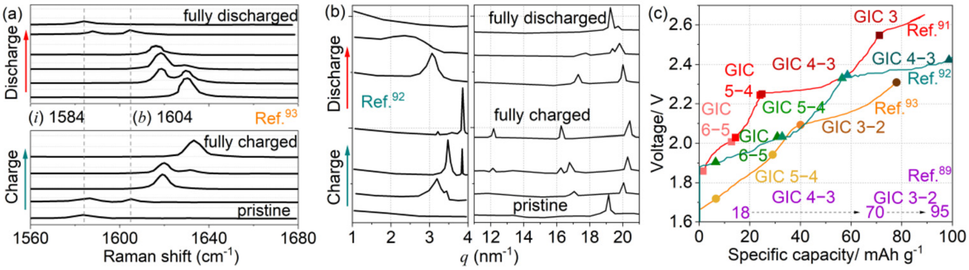

Fig. 11 (a) Selected *in situ* Raman spectra of the graphite electrode recorded during charge/discharge at 50 mA g^{-1}.[93] (b) Selected SAXS (left) and WAXS (right) profiles of the first cycle along with charge/discharge at 50 mA g^{-1}.[92] (c) The relative specific capacity across intercalation stages during the first cycle based on publication: galvanostatic charging curve (25 mA g^{-1}) of Swagelok type cell[89] and PEEK self-made cell[92] with $AlCl_3$/[EMIM]Cl (1.5 : 1) electrolyte, galvanostatic charging curve (50 mA g^{-1}) of pouch cell with $AlCl_3$/[EMIM]Cl (1.7 : 1) at −10 °C,[91] and galvanostatic charging curve (50 mA g^{-1}) of pouch cell with $AlCl_3$/urea (1.3 : 1) electrolyte.[93] Adapted from Elia, G. A. *et al.*, *Adv. Funct. Mater.*[89] Licensed under CC BY. ©2020 Wiley. Adapted with permission from author. Copyright 2018.[91] Adapted from Greco, G. *et al.*, Small Methods.[92] Licensed under CC BY 3.0. ©2021 Wiley. Adapted with permission from author.[93] Copyright 2017.

erature is lowered to −10 °C, a stage 3 GIC can form at 2.6 V, and further cooling to −40 °C results in the formation of a stage 3 GIC at a slightly lower voltage of 2.5 V. This behavior is attributed to temperature-insensitive distributions,[94] which suggest that factors such as fast ion diffusion, low interfacial resistance, and high availability of active species in the double layer contribute to the unexpectedly high-rate performance at low temperatures. This is particularly noteworthy since, in most systems, lower temperatures typically reduce ion mobility and intercalation efficiency.

In contrast, Greco *et al.*[86] calculated a stage 4 GIC in the fully charged state at 2.4 V through *ex situ* measurements using the following equation:

$$\Delta d = I_\mathrm{c} - 0.335n = d_\mathrm{i} - 0.335(n+1)$$

where Δd is the gallery expansion, I_c is the periodic repeat distance measured using SAXS, 0.335 (nm) is the lattice parameter of graphite and n is the intercalation stage. Later, they investigated the mechanism through *operando* X-ray scattering from small angles to wide angles, which indicates a gradual shift from stage 6 to 3 when fully charged to 2.4 V.[92] Fig. 11b presents part of the SAXS and WAXS profiles. During charging, a gradual shift of the peak, and a switch of the peaks located at 3.2 $\mathrm{nm^{-1}}$ and 4 $\mathrm{nm^{-1}}$ were observed in the SAXS spectra. Besides, the (002) reflection of graphite in the WAXS spectra disappears alongside the formation of two new reflections associated with the formation of the GIC. When fully discharged, it is highly symmetric with the charging process, demonstrating complete reversibility of the process. Wang *et al.*[87] found a stage 3 GIC when fully charged to 2.45 V, and the interlayer space of graphene expanded to 9.22 Å as seen in the *in situ* XRD measurement. In addition, the reversible discharge capacity of the battery at higher temperatures was found to be superior to that of room temperature. A higher discharge capacity can be obtained at increased temperatures (*i.e.* moderate 40 °C).[95] This can be attributed to the fact that higher temperature accelerates the diffusion and transmission of anions in the electrolyte, facilitating the intercalation/deintercalation in graphitic carbons.

Overall, there is a lack of consistency in the reported stage number of fully charged intercalation compounds across various studies, as shown in Fig. 11c. One key factor contributing to this discrepancy is the preferential intercalation that occurs at the surface of the cathode, rather than throughout the bulk. Surface-sensitive techniques, such as Raman spectroscopy, tend to detect higher degrees of intercalation, often corresponding to lower stage indices (*e.g.*, stage 1 or 2 GICs) under fully charged conditions. In contrast, bulk-sensitive methods like XRD, which probe deeper into the material, typically observe lower intercalation levels, corresponding to higher stage indices (*e.g.*, stage 3 or 4 GICs). This discrepancy underscores the importance of combining both surface and bulk characterization methods to achieve a more comprehensive and accurate understanding of the intercalation behavior in these materials. Beyond the choice of technique, factors such as porosity, applied voltage, temperature, and electrolyte composition also influence the degree of anion intercalation into graphite. Higher porosity creates more pathways for ion diffusion, while the applied voltage governs the electrochemical driving force for intercalation, with higher voltages promoting greater ion insertion but potentially causing instability at extreme levels. Both lower and potentially higher temperatures were found to improve performance in specific systems, but the underlying mechanisms need to be carefully optimized for stability and capacity. Additionally, electrolyte composition affects the availability and mobility of ions, with different electrolytes influencing the efficiency and stability of the intercalation process. Furthermore, meaningful comparisons of GIC levels across studies are hindered by variations in both the types of materials and the volumes employed.

A survey of recent work on graphitic carbon and hard carbon cathodes of AGDIBs is listed in Table 2. The best electrochemical performance in each year is compared. Generally, the specific capacities obtained for graphitic materials are mostly around 100 mAh $\mathrm{g^{-1}}$ and not more than 150 mAh $\mathrm{g^{-1}}$, but high rates and ultra-long-term cycling life are achieved. In hard carbon, the specific capacity reaches above 400 mAh $\mathrm{g^{-1}}$; however, only under lower current densities. Graphitization degree, defects, pore structures, and morphology play crucial roles in affecting electrochemical performance. Fast electron transportation is based on a high graphitization degree, while hetero atoms doping offers more active sites for surface adsorption of $\mathrm{AlCl_4^-}$. Thus, defect-free few-layer graphene demonstrated the best high-rate performance. Hard carbon, especially containing heteroatoms, displayed the highest specific capacities. The pore size as well as the interlayer space need to be big enough for the intercalation of $\mathrm{AlCl_4^-}$ anions but avoid a large accumulation of ions in too big spaces. Particularly, taking advantage of unique morphologies (flakes/microflowers/open nanostructures) may result in a higher capacity and rate performance.

Overall, it requires a high graphitization degree, defect-free planes, high porosity, and high stability for graphitic materials to deliver optimal performance. However, it is important to note that the current cathode capacity of such materials may be approaching its maximum, limiting the potential for significant increases in energy density. Hard carbon exhibits a notably high specific capacity but suffers from limited rate capability, likely due to either (i) slow charge storage kinetics or (ii) different storage mechanisms compared to graphitic materials. This performance difference may stem from its unique properties, such as an amorphous microstructure, abundant defect sites, and complex pore networks that simultaneously enable high capacity while restricting rapid ion transport. To advance the development of high-performance AGDIBs, future studies should focus on two key objectives:

(1) Optimization of graphitic carbon cathodes for high-power applications

- Design strategies to enhance fast ion transport kinetics.
- Investigate electrolyte formulations that enable rapid anion intercalation.

(2) Fundamental understanding of hard carbon storage mechanisms

Table 2 A comparison of electrochemical performance of various cathode materials of AGDIBs over the years

			Long-term cycling				
Cathode	Electrolyte	Specific capacity (mAh g^{-1})/current density (mA g^{-1})	Specific capacity (mAh g^{-1})	Current density (mA g^{-1})	Capacity retention	Cycle number	Year Ref.
Graphite/few-layer graphene							
Reduced graphene oxide	$AlCl_3$/[EMIm]Cl 1.3 : 1	149/500	94.5	5000	95.8%	10 000	2025 [96]
Recycled graphite	$AlCl_3$/[EMIm]Cl 1.3 : 1	138/2000	127	10 000	97.0%	2000	2024 [59]
Kish-based expanded graphite	$AlCl_3$/[EMIm]Cl no ratio	141/50	134	1000	99.1%	10 000	2024 [17]
Modified expanded graphite	$AlCl_3$/[EMIm]Cl 1.3 : 1	118/1000	102	5000	100.0%	10 000	2023 [97]
Free-standing expanded graphite film	$AlCl_3$/Et_3NHCl 1.5 : 1	110/1000	100	5000	—	27 500	2022 [67]
Graphene nanoplatelets	$AlCl_3$/TMAHCl 1.7 : 1	134/2000	134	2000	98%	3000	2020 [98]
Natural graphite powder	$AlCl_3$/[EMIm]Cl no ratio	100/1000	~60	20 000	70.0%	500 000	2019 [5]
Nanosheet-bricked porous graphite	$AlCl_3$/[EMIm]Cl 1.3 : 1	103/2000	104	10 000	—	3000	2018 [66]
Carbon nanoscrolls	$AlCl_3$/[EMIm]Cl 1.3 : 1	104/1000	101	50 000	100.0%	55 000	2018 [69]
Edge-rich few-layer graphene	$AlCl_3$/[EMIm]Cl 1.3 : 1	128/2000	90	8000	99.2%	20 000	2018 [72]
Defect-free few-layer graphene	$AlCl_3$/[EMIm]Cl 1.3 : 1	100/5000	97	50 000	97.0%	25 000	2017 [77]
"3H3C" graphite	$AlCl_3$/Et_3NHCl 1.5 : 1	116/300 000	120	400 000	91.7%	250 000	2017 [4]
Hard carbon							
N-doped hard carbon	$AlCl_3$/[EMIm]Cl 1.3 : 1	323/500	109	1000	—	1000	2024 [80]
Layered N,S-doped carbon	$AlCl_3$/[EMIm]Cl no ratio	330/500	90	5000	97.0%	10 000	2024 [81]
Pomegranate peel-based carbon	$AlCl_3$/[EMIm]Cl 1.3 : 1	125/200	82	150	—	500	2023 [99]
Coconut shell-based porous carbon	$AlCl_3$/[EMIm]Cl 1.3 : 1	150/100	~80	1000	90.0%	1500	2022 [100]
N,P-doped carbon	$AlCl_3$/[EMIm]Cl 1.3 : 1	110/500	98	5000	~100%	2500	2018 [82]

- Utilize advanced *in situ*/*operando* characterization techniques to uncover the dominant charge storage processes. A combined approach using both surface-sensitive (*e.g.*, XPS, Raman) and bulk-sensitive (*e.g.*, XRD, neutron scattering) methods is essential to capture the complex interfacial and structural evolution occurring during cycling.
- Establish correlations between material properties (porosity, heteroatom doping, defect density) and electrochemical performance.
- Develop quantitative models to distinguish between intercalation, adsorption, and pore-filling contributions.

This dual-focused approach will drive the design of next-generation carbon materials, combining the high-rate capability of graphitic structures with the exceptional capacity of optimized hard carbons.

4. Electrolytes

The choice of electrolyte is critical, as it must facilitate efficient ion transport while functioning as both anolyte and catholyte. Even though research on AGDIBs electrolytes started from inorganic molten salts, high operation temperatures significantly hindered their application.[101] Various alternative electrolytes have been explored to further enhance performance and stability, offering potential improvements in efficiency, cycling life, and overall battery characteristics. Based on a survey of publications from the past decade, $AlCl_3$/[EMIm]Cl is the most widely used electrolyte in AGDIBs, accounting for around 67% of applications. It is followed by $AlCl_3$/Et_3NHCl (approximately 10%), $AlCl_3$/urea (around 3%), and various other alternatives (about 20% in total). Among these, $AlCl_3$/[EMIm]Cl is typically chosen as a benchmark for comparison due to its established performance and widespread adoption in research and development. However, its highly acidic nature and associated corrosion issues have raised significant concerns, prompting studies on alternative systems. Recent advances in electrolyte research have mainly focused on three directions: ionic liquid (IL) electrolytes, deep eutectic electrolytes (DEE), and gel polymer electrolytes.

4.1 ILs

Due to the robust thermal stability, high ionic conductivity, low volatility, non-flammability and wide electrochemical window, ILs have been extensively investigated in AGDIBs. As the most popular IL electrolyte, $AlCl_3$/[EMIm]Cl has a high ionic conductivity of 10–20 mS cm^{-1} at room temperature, but this value varies according to the ratio between $AlCl_4^-$ and $Al_2Cl_7^-$.[102,103] It has a melting point of −80 °C and exhibits stability at temperatures up to 95 °C.[104] Its wide electrochemical stability window (approximately −2.0—2.4 V *vs.* Al/Al^{3+})[105] enables this material to serve as a suitable electrolyte, without significant oxidative or reductive degradation during cycling (typically 0.5—2.37 V *vs.* Al/Al^{3+}).[98] However, this electrolyte is hygroscopic, and moisture can decompose it or decrease its potential window. For example 3 wt% of water could decrease the anodic and cathodic potential window from 6 V to 3 V.[106] Furthermore, the carrier ions in $AlCl_3$/[EMIm]Cl are $AlCl_4^-$ and $Al_2Cl_7^-$ rather than Al^{3+}.[107] Subsequently, the energy storage is based on a dual-ion mechanism, $AlCl_4^-$ anion intercalation/deintercalation into the graphite cathode and Al plating/stripping on the Al anode.[22] Herein, ILs used in AGDIBs are not just electrolytes (ion-conductors) but represent an electrochemically active, capacity- and rate-limiting battery component.[21]

It is essential to know that the Al deposition which takes place at the existence of $Al_2Cl_7^-$ ions can only occur in acidic

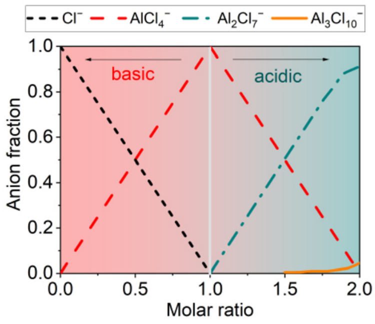

Fig. 12 The anion speciation diagram of $AlCl_3$/[EMIm]Cl at room temperature, illustrating the electrolyte compositions at $0 < r < 2$. Adapted from Palacin, M. R. *et al.*, *J. Phys.: Energy*.[107] Licensed under CC BY 4.0. ©2024 IOP Publishing.

conditions.[107] Hence, the storage performance is highly dependent on the molar ratio (r) of $AlCl_3$ to [EMIm]Cl. The anion speciation diagram of $AlCl_3$/[EMIm]Cl is shown in Fig. 12. First, r should be above 1.0 so that an acidic condition is maintained. Besides, 2.0 is the highest value for this electrolyte to remain completely in a liquid phase. Note that, the ratio value is strongly related to the theoretical energy density of electrolyte; at ratio values of 2.0 and 1.3, the theoretical energy densities are 65–70 Wh kg^{-1} and 33 Wh kg^{-1}, respectively.[108] $AlCl_3$/[EMIm]Cl (2.1 : 1) utilizing an excess of $AlCl_3$ was reported.[109] The battery possesses a high energy density of 59.1 Wh kg^{-1}, cathodic capacity of 103 mAh g^{-1}, and an average discharge voltage of 1.71 V. Nevertheless, an excess amount of $AlCl_3$ crystallized in the glass fiber separator. Moreover, the higher the ratio, the more acidic the electrolyte becomes, making it highly corrosive to conventional battery components.[110] A molar ratio of 1.3 provides an optimal balance of $AlCl_4^-$ and $Al_2Cl_7^-$, enabling efficient and reversible aluminum deposition while minimizing corrosion. Higher ratios increase acidity and $Al_2Cl_7^-$ concentration, which can compromise electrode stability and long-term cycling. Consequently, a ratio of 1.3 is most commonly employed in research, with 1.5 used less frequently.

The practical application of $AlCl_3$/[EMIm]Cl is limited by its high cost, hygroscopicity, leakage risk, and strong corrosivity. To address these issues, alternative electrolytes have been investigated, primarily to verify stable Al deposition. One approach involves $AlCl_3$-based ionic liquids prepared with cheaper Lewis basic ligands. For example, $AlCl_3$/1-butyl-3-methylimidazolium chloride ([BMIm]Cl) enables AGDIB operation at subzero temperatures, with no phase transitions observed between 0 and −35.5 °C during heating or cooling.[111] However, compared to $AlCl_3$/[EMIm]Cl, this electrolyte exhibits a lower diffusion coefficient of $Al_2Cl_7^-$ due to higher viscosity, and the resulting thicker Al deposits promote dendrite formation.[112,113] Another strategy is to use mixtures of organic cations to disrupt ion cluster formation and enhance ion mobility. In $AlCl_3$–[EMIm]Cl/[BMIm]Cl (2 : 1), the battery showed improved low-temperature performance, with specific capacity retention increased by 24% at −20 °C and 9% at −40 °C relative to $AlCl_3$/[EMIm]Cl.[114]

In addition, triethylamine hydrochloride (Et_3NHCl)-based electrolytes derived from otherwise intractable industrial waste have also attracted increasing attention. These electrolytes are considered highly valuable due to their extremely low cost—potentially thousands of times cheaper than [EMIm]Cl—while still supporting reversible Al electrochemistry.[20] An $AlCl_3$/Et_3NHCl (1.7 : 1) electrolyte shows a high ionic conductivity of 13.5 mS cm^{-1}.[115] Most importantly, both $AlCl_4^-$ and $Al_2Cl_7^-$ anions have been detected in $AlCl_3$/Et_3NHCl.[12] Mukundan *et al.*[116] stated that the ratio of the concentrations of $AlCl_4^-$ to $Al_2Cl_7^-$ ions (denoted as $n(AlCl_4^-)/n(Al_2Cl_7^-)$) equals 1 in both $AlCl_3$/Et_3NHCl (1.5 : 1) and $AlCl_3$/[EMIm]Cl (1.5 : 1) electrolytes. They further observed that, during long-term cycling, the potential of the Al anode decreases and the morphology of the graphite matrix evolves, leading to an impressive 52% increase in specific capacity for cell with $AlCl_3$/Et_3NHCl compared to $AlCl_3$/[EMIm]Cl electrolytes. Moreover, a reduced self-discharge capacity loss of 3% (instead of 10%) within 24 h was achieved using $AlCl_3$/Et_3NHCl electrolyte and glassy carbon current collector.[26] As shown in Fig. 13a, the CVs of cell with $AlCl_3$/Et_3NHCl and $AlCl_3$/[EMIm]Cl electrolytes show similar

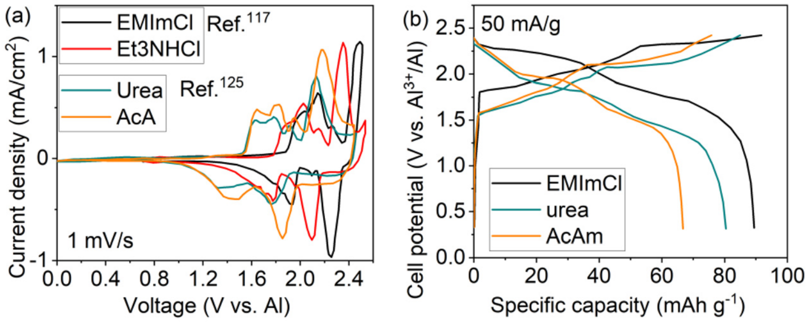

Fig. 13 (a) CV curves of Al//expanded graphite cells with $AlCl_3$/[EMIm]Cl and $AlCl_3$/Et_3NHCl electrolytes[117] and Al//natural graphite cells employing $AlCl_3$/urea and $AlCl_3$/AcA electrolytes[125] (molar ratio 1.5 : 1) at a scan rate of 1 mV s^{-1}. (b) Charge/discharge profiles of Al//natural graphite cells with $AlCl_3$/[EMIm]Cl, $AlCl_3$/urea and $AlCl_3$/AcA electrolytes (molar ratio 1.5 : 1) at a current density of 50 mA g^{-1}.[125] Adapted with permission from Elsevier.[117] Copyright 2019. Adapted with permission from Wiley.[125] Copyright 2021.

peaks, but the redox signals of the one with $AlCl_3/Et_3NHCl$ are shifted to lower potentials, indicating that the $AlCl_4^-$ intercalation into the graphite interlayer in $AlCl_3/Et_3NHCl$ electrolyte is stronger than in $AlCl_3$/[EMIm]Cl electrolyte.[117] Xu *et al.*[20] found that $AlCl_3/Et_3NHCl$ electrolyte showed a higher decomposition voltage, implying a wider potential window for AGDIBs. The cell could run under an upper cut-off voltage of 2.62 V with an CE of 96% over 6000 cycles, while the CE drops significantly to 89% when using $AlCl_3$/[EMIm]Cl electrolyte. A similar cost-effective electrolyte, $AlCl_3$/trimethylamine hydrochloride (TMAHCl), was also studied in AGDIBs. At a ratio above 1.6 : 1, the ionic conductivity of $AlCl_3$/TMAHCl is close to $AlCl_3$/[EMIm]Cl and $AlCl_3/Et_3NHCl$ at the same ratio (Fig. 15a). It endowed the cell to operate across temperatures ranging from −10 °C to 60 °C, and a full battery with $AlCl_3$/TMAHCl (1.7 : 1) electrolyte was estimated to deliver a higher cell-level specific capacity than $AlCl_3/Et_3NHCl$ and $AlCl_3$/[EMIm]Cl.[98] However, the ionic conductivity and electrochemical performance of this electrolyte at ratios below 1.6 have not been provided, making it difficult to compare with other electrolytes at their typical ratios. Additionally, this electrolyte has not been further studied in any other reports. Consequently, $AlCl_3$/[EMIm]Cl remains the benchmark electrolyte due to its well-balanced properties; $AlCl_3/Et_3NHCl$ is gaining popularity as a lower-cost alternative. Nevertheless, researchers often continue using familiar systems ($AlCl_3$/[EMIm]Cl), highlighting that practical adoption depends not only on raw performance but also on the challenges of modifying long-established electrochemical protocols.

4.2 DEEs

DEEs have attracted particular interest in AGDIBs due to their non-flammability, non-toxicity, inexpensiveness, facile synthesis, as well as remarkable electrochemical stability. In 2015, for the first time, a mixture of $AlCl_3$ and urea in a 1.3 : 1 molar ratio was reported by Angell *et al.*[93] They found that several graphite oxidation peaks and the corresponding reduction peaks in CV curves were easily correlated with the galvanostatic charge/discharge curve, indicating good reversibility. Previously, it was believed that, in an $AlCl_3$/urea electrolyte, Al plating/stripping proceeds through two pathways, namely reactions of electroactive anionic ($Al_2Cl_7^-$) and cationic ($AlCl_2\cdot(urea)_2^+$) species,[118] where the cationic one dominates. However, later, *operando* Raman spectroscopy of the Al plating/stripping process revealed a large decrease in the $Al_2Cl_7^-$ peak (313 cm^{-1}) and a corresponding increase in the $AlCl_4^-$ peaks (350 and 445 cm^{-1}).[119] These results strongly suggest that deposition at the Al anode primarily proceeds *via* $Al_2Cl_7^-$ and the $AlCl_4^-$ intercalation at the cathode in $AlCl_3$/urea follows the same mechanism as in $AlCl_3$/[EMIm]Cl.

However, $AlCl_3$/urea has higher viscosity (88.9 mPa s^{-1} at $r = 1.5$) and low conductivity (1.17 mS cm^{-1} at $r = 1.5$),[119] which limits its performance at room temperature. Increasing the $AlCl_3$-to-urea molar ratio or operating at elevated temperatures can improve electrochemical behavior,[120] but such conditions are generally impractical for standard battery applications. The battery capacity with an $AlCl_3$/urea electrolyte was reported to be much lower than the one with $AlCl_3/Et_3NHCl$ electrolyte.[115] Applying $AlCl_3$/urea derivatives (*e.g. N*-methyl urea (Me-Ur) and *N*-ethyl urea (Et-Ur)) was found to greatly reduce the viscosity (by a factor of three) and increase ionic conductivity (by 40%), leading to improved coulombic efficiencies.[119] Ternary electrolytes in proper molar ratios show improved performance. The battery performance with ternary $AlCl_3$/Urea/[EMIm]Cl ($13.5 : 9 : X$, X = 0, 0.6, 0.8, 1) electrolyte is improved with increasing [EMIm]Cl content.[121] *In situ* XRD confirmed $AlCl_4^-$ intercalation/deintercalation in graphite, but the broad shoulder of the peak of the fully discharged graphite indicates residual disorder and strain. Furthermore, the impact of the electrolyte composition on the Al electrodeposition mechanism has been analyzed.[122] Decreasing the [EMIm]Cl concentration in ternary $AlCl_3$/[EMIm]Cl/urea ($60 : 40 - X : X$) electrolytes causes uniformly electrodeposited Al crystals to grow larger. When $X \geq 30$, Al nanoplatelets (width of 10–15 μm) oriented in the (111) direction spontaneously formed. A small amount of urea in $AlCl_3$/Urea/[EMIm]Cl ($1.3 : X : 1 - X$, X = 0.25) greatly improved Al platting/stripping down to −40 °C.[123] $AlCl_3$/urea/caprolactam(CPL) was applied in AGDIBs, achieving a high initial specific capacity of 151 mAh g^{-1} at 5000 mA g^{-1} and retained 132 mAh g^{-1} after 3000 cycles.[124] Cells with an $AlCl_3$/acetamide (AcA) electrolyte were found to exhibit very similar peaks to the $AlCl_3$/Urea electrolyte in CV plots (Fig. 13a).[125] The redox signals of $AlCl_3$/AcA shifted to lower potentials compared to $AlCl_3$/Urea, corresponding to lower potential plateaus during charging/discharging (Fig. 13b). However, cells with $AlCl_3$/AcA present a much lower specific capacity in comparison to $AlCl_3$/urea in AGDIBs. Incorporating an F-substituted AcA additive into the $AlCl_3$/AcA electrolyte can induce the formation of an F-rich interphase layer, which stabilizes Al plating/stripping and accelerates its kinetics.[126] On the contrary, a comparative study revealed that a cell with $AlCl_3$/AcA possessed a higher specific capacity than the one with commercial $AlCl_3$/[EMIm]Cl,[127] highlighting the importance of standardized testing conditions for objective electrolyte evaluation.

Fig. 14a and b compare the oxidation potential of various aluminate chloride-containing electrolytes and the specific capacity in Al//graphite full cells, respectively. The decomposition voltage of these electrolytes (including $AlCl_3$/[EMIm]Cl) is generally below 2.5 V, except $AlCl_3$/AcA with a dFAcA additive (2.78 V), $AlCl_3$/[EMIm]Cl with an LiBOB additive (2.74 V), $AlCl_3$/[BMP]Cl (2.83 V), and $AlCl_3$/[BMIm]Cl (2.5–2.6 V depends on the molar ratio and temperature). The additives render electrolytes more stable at higher voltage, which benefits battery performance. Though $AlCl_3$/AcA + dFAcA was only tried in an Al//sulfur cell, the existence of $Al_2Cl_7^-$ and $AlCl_4^-$ anions should allow its application in AGDIBs. $AlCl_3$/[BMP]Cl shows the highest voltage, unfortunately, the full cell specific capacity was found to be 0 because of the inability of Al electrodeposition. $AlCl_3$/urea/CPL delivers the highest specific capacity, which may be due to its higher concentrations of $Al_2Cl_7^-$ and $AlCl_4^-$ anions. However, the electrochemical performance

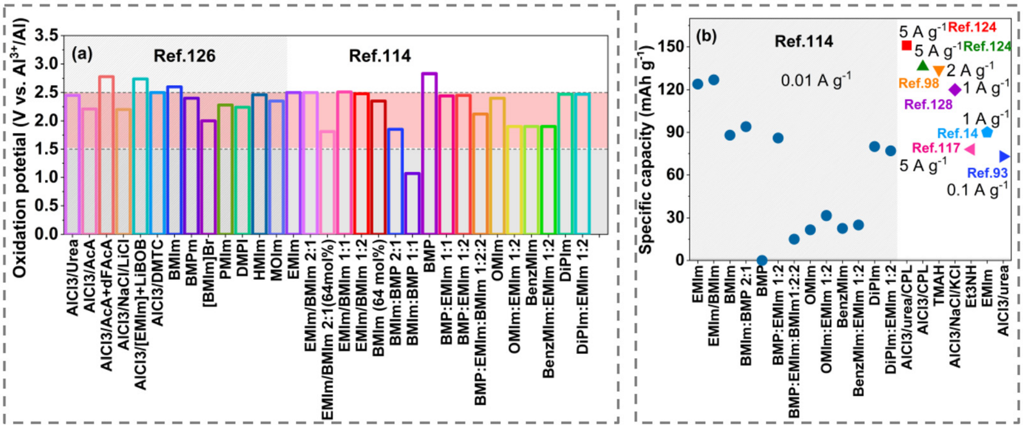

Fig. 14 (a) The oxidation onset potentials of various $AlCl_3$/[X]Cl and other alternative electrolytes.[114,126] (b) Specific capacities of Al/graphite cells with various $AlCl_3$/[X]Cl and other alternative electrolytes. $AlCl_3$/[X]Cl (X = EMIm to DiPIm : EMIm 1 : 2) at 0.01 A g^{-1},[114] $AlCl_3$/urea/CPL and $AlCl_3$/CPL at 5 A g^{-1},[124] $AlCl_3$/TMAHCl at 2 A g^{-1},[98] $AlCl_3$/NaCl/KCl at 1 A g^{-1},[128] $AlCl_3$/Et_3NHCl at 5 A g^{-1},[117] $AlCl_3$/[EMIm]Cl at 1 A g^{-1},[14] and $AlCl_3$/urea at 0.1 A g^{-1}.[93] Adapted with permission from American Chemical Society.[114] Copyright 2023. Adapted with permission from John Wiley and Sons.[126] Copyright 2023.

depends not only on the electrolyte but also on various cell parameters. Therefore, differences in performance between studies may not only result from the electrolyte but also from the use of different cell components and configurations.

Since the corrosive nature of electrolytes is primarily caused by $Al_2Cl_7^-$ ions, some researchers have attempted to explore Cl-free electrolytes. Particularly, aluminum trifluoromethanesulfonate ($Al(OTF)_3$)–based electrolytes, which may be capable of fast Al^{3+} transport and reduced corrosivity, have been investigated. Unfortunately, it was found that these non-corrosive electrolytes lead to unexpected challenges related to the reversibility of the redox reactions.[129] No Al plating/stripping occurs on the Al electrode, which is believed probably due to the low corrosivity and the resulting inability to consume the Al_2O_3 passivation layer.[130,131] Wang *et al.*[132] found pitting corrosion of the Al foil in an $Al(OTF)_3$–based electrolyte after it had been previously immersed in an $AlCl_3$/[BMIm]Cl (1.1 : 1) electrolyte; however, no evidence was provided regarding the Al plating/stripping process. Overall, Cl-free electrolytes offer a promising route toward addressing the corrosivity of electrolytes, although significant challenges remain regarding the reversibility of Al plating/stripping.

Recently, a low-cost, non-corrosive, and air-stable, chloride-free Al-based hydrated eutectic electrolyte was synthesized composed of aluminum perchlorate nonahydrate ($Al(ClO_4)_3{\cdot}9H_2O$) and methyl urea (MU) ligand.[133] The stability of Al plating/stripping was evaluated in symmetrical cells. The cell ran over 150 h with a steady voltage hysteresis, and the formation of Al deposits was observed on the surface of the Al foil after cycling. In addition, a symmetrical cell with two pieces of titanium (Ti) metallic foil was assembled to further evaluate Al plating. Al uniformly distributed on the cycled Ti electrode, confirming the Al deposition. Although this electrolyte was only utilized in Al//V_2O_5 full cells, its potential application in AGDIBs is worth further exploration.

From an experimental perspective, in most cases, a comparison to $AlCl_3$/[EMIm]Cl under the same battery conditions has not been conducted, hence making it difficult to identify the advantages of alternative electrolytes. According to a literature survey on the pretreatment of electrolytes for AGDIBs, to date, only 1% dried and purified electrolytes before cell assembly, 20% only dried but not purified, and surprisingly 80% without mentioning this process. Obviously, the conditions of electrolytes, specifically moisture and purity, have significant impacts on cell performance. Therefore, careful attention to the electrolyte preparation is essential. Highly acidic electrolytes can corrode cell components, while the concentration of acidic anions may limit capacity, making it crucial to achieve a balanced formulation for optimal performance. The development of low-cost, high-performance electrolytes—particularly those that are non- or less corrosive—remains a key research priority.

4.3 Gel polymer electrolytes

A gel polymer electrolyte is typically prepared by encapsulating or immobilizing ionic liquids within a polymer matrix. This approach effectively mitigates the risk of corrosion, reduces moisture sensitivity, and opens the possibility of eliminating conventional glass fiber separators, enabling the development of flexible batteries. In 2016, for the first time, a gel polymer electrolyte ($AlCl_3$/[EMIm]Cl-PAM) was successfully prepared *via* free radical polymerization, using $AlCl_3$ complexed acrylamide to prepare the polymer matrix (PAM) and $AlCl_3$/[EMIm]Cl as the functional IL.[134] Al deposition was achieved; however, the ionic conductivity of this electrolyte was found to be too low (1.66 mS cm^{-1}) compared to other reported electrolytes (Fig. 15a). Yu *et al.*[135] applied $AlCl_3$/[EMIm]Cl-PAM in an Al//graphite cell, achieving a specific capacity of ~120 mAh g^{-1} at a relatively low current density of 60 mA g^{-1}. The gel polymer electrolyte exhibited excellent safety: no leakage was observed,

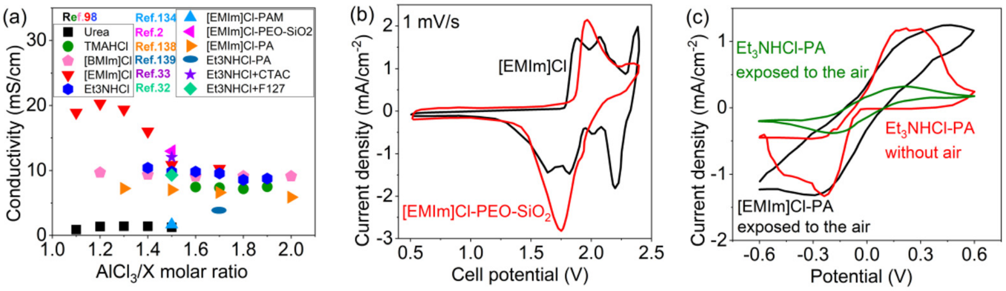

Fig. 15 (a) Ionic conductivity of various $AlCl_3$/X electrolytes. X = [EMIm]Cl (10–20 mS cm^{-1}), TMAHCl (average ~7.5 mS cm^{-1}), Et_3NHCl (~9.6 mS cm^{-1}), [BMIm]Cl (~9.4 mS cm^{-1}), and urea (~1.3 mS cm^{-1}) were measured at 25 °C.[98] [EMIm]Cl-PAM (1.66×10^{-3} S cm^{-1}, measured at 20 °C) is gel polymer electrolyte made from $AlCl_3$ complexed acrylamide and $AlCl_3$/[EMIm]Cl (1.5 : 1).[134] [EMIm]Cl-PEO-SiO_2 (13 mS cm^{-1}) is gel polymer electrolyte made from PEO, $AlCl_3$/[EMIm]Cl (1.5 : 1) and an additive-fumed SiO_2.[2] [EMIm]Cl-PA (5.89 to 7.24 mS cm^{-1}, measured at room temperature) and Et_3NHCl-PA (3.86 mS cm^{-1}, measured at 25 °C) is PA-based gel polymer electrolyte made with $AlCl_3$/[EMIm]Cl (2 : 1 to 1.3 : 1)[138] and $AlCl_3/Et_3NHCl$ (1.7 : 1),[139] respectively. $AlCl_3/Et_3NHCl$ (1.5 : 1) add CTAC (12.06 mS cm^{-1})[33] and F127 (9.31 mS cm^{-1})[32] are named Et_3NHCl + CTAC and Et_3NHCl + F127, respectively. (b) CV curves of Al//natural graphite cells with $AlCl_3$/[EMIm]Cl and $AlCl_3$/[EMIm]Cl-PEO-SiO_2 electrolytes showing anions intercalation at a scan rate of 1 mV s^{-1}. Adapted from Leung, O. M. *et al.*, *Adv. Energy Mater.*[2] Licensed under CC BY 3.0. ©2024 John Wiley and Sons. (c) CV curves of Al//natural graphite cells with $AlCl_3$/[EMIm]Cl-PA[138] (not mentioning the scan rate) and $AlCl_3/Et_3NHCl$-PA[139] (without air not mentioning the scan rate, and after being exposed to the air for 10 min at a scan rate of 1 mV s^{-1}) presenting Al plating/stripping. Adapted with permission from Elsevier.[138] Copyright 2021. Adapted with permission from American Chemical Society.[139] Copyright 2021.

and even after cutting off a portion of the cell, the connected LED continued to operate without disruption. Remarkably, the battery remained functional when combusted, powering the LED without flames or explosions. *In situ* XRD and *in situ* Raman spectra revealed the reversible anion intercalation into the graphite cathode. By using acrylamide to form a polymer matrix, they also studied $AlCl_3/Et_3NHCl$-PAM.[136] It achieved stable potential curves even upon bending, enhanced moisture resistance, and a high decomposition voltage of 2.96 V. The corresponding Al//graphite cell demonstrated stable performance, delivering a discharge capacity of 91 mAh g^{-1} at a current density of 1000 mA g^{-1}. While current studies have validated cycle life up to 800 cycles, long-term data (>2000 cycles) remains unavailable and is crucial for assessing their practical deployment viability.

Schoetz and coworkers[137] found that Al can be deposited from a Lewis neutral ion gel (based on polyethylene oxide (PEO) and $AlCl_3$/[EMIm]Cl) without any dendrite growth within a wide potential stability window of 5 V. Building on this, a solid polymer electrolyte was fabricated using a solvent-free method with PEO, $AlCl_3$/[EMIm]Cl (molar ratio = 1.5), and an additive-fumed silicon dioxide (SiO_2).[2] This electrolyte ($AlCl_3$/[EMIm]Cl-PEO-SiO_2) maintained a high ionic conductivity of 13 mS cm^{-1}, which is higher than $AlCl_3$/[EMIm]Cl (Fig. 15a). When the charging cut-off potential is increased to 2.8 V, the specific capacity increases by approximately 48%, reaching 194 mAh g^{-1} after three cycles representing a 58% improvement compared to the ionic liquid. Meanwhile, due to the decreased ion mobility, the CV curves of the cells with $AlCl_3$/[EMIm]Cl-PEO-SiO_2 do not exhibit distinct redox peaks, unlike those of $AlCl_3$/[EMIm]Cl (Fig. 15b).

Polyamide (PA), another efficient polymer, was used as the polymer matrix for $AlCl_3$/[EMIm]Cl and $AlCl_3/Et_3NHCl$ ILs. During the fabrication of the gel polymer electrolyte, the strong hydrogen bonds in the PA chains are initially broken down in ILs and then reorganize into a configuration where the molecules are connected, increasing the polymer's flexibility. $AlCl_3$/[EMIm]Cl-PA with an ionic conductivity of 6.61 mS cm^{-1} was prepared through a solvent-free procedure enabling the Al//graphite cells to cycle well in a wide temperature range from −30 °C to 45 °C.[138] Simply adding PA into the acidic $AlCl_3/Et_3NHCl$ through stirring and heating, a $AlCl_3/Et_3NHCl$-PA was obtained after cooling.[139] However, the ionic conductivity of $AlCl_3/Et_3NHCl$-PA is slightly lower than $AlCl_3$/[EMIm]Cl-PA at the same IL molar ratio (Fig. 15a). After being exposed to air, reversible Al plating/stripping was still observed in both $AlCl_3/Et_3NHCl$- and $AlCl_3$/[EMIm]Cl-PA gel polymer electrolytes (Fig. 15c). The Al//graphite cell demonstrated excellent interfacial stability, operating for over 3800 hours. Remarkably, even when partially severed, the remaining section was still capable of lighting a red LED lamp—despite being folded—without any electrolyte leakage. *In situ* XRD analysis revealed the presence of a stage 3 GIC at the fully charged state. The melt flow index of the PA-based $AlCl_3/Et_3NHCl$ gel polymer electrolyte increased nearly linearly with $AlCl_3$ concentration, indicating reduced molecular cohesion. This behavior likely arises from the preferential formation of bidentate coordination between Al atoms and the O and N atoms in the polymer, which suppresses interchain hydrogen bonding and lowers cohesion.[140] As a result, PA-based gel polymer electrolytes significantly improve cell stability by enhancing moisture resistance and reducing the risk of leakage and corrosion.

In terms of ionic conductivity, polymer matrices based on PEO and PA outperform those using acrylamide. While gel polymer electrolytes address key safety concerns, their performance is still limited by a narrow operational window at higher current densities. For practical implementation in high-power systems, substantial improvements in electrochemical

Table 3 Summary of electrolytes employed in A//graphite battery over time

Electrolyte	Ionic conductivity	Test voltage range	Cell performance (mAh g^{-1}/mA g^{-1}, capacity retention after cycles)	Year [Ref.]
ILs and DEEs				
$AlCl_3$/urea/[EMIm]Cl 1.3 : 0.25 : 0.75	—	0.2 V to 2.4 V	110/60	2024 [123]
$AlCl_3$/acetamide 1.4 : 1	—	0.3 V to 2.4 V	101/50; 80/500, 92% retention after 1000 cycles	2024 [127]
$AlCl_3$/Et_3NHCl 1.5 : 1	10 mS cm^{-1} (ref. 98)	0.5 V to 2.5 V	94.2/1000, 157% retention after 1000 cycles	2023 [116]
$AlCl_3$/[EMIm]Cl–[BMIm]Cl 2 : 1	13.8 mS cm^{-1}	0.5 V to 2.45 V	125/10	2023 [114]
$AlCl_3$/urea 1.5 : 1	1.3 mS cm^{-1} (ref. 98)	0.3 V to 2.4 V	50/2000, 80% retention after 8000 cycles	2021 [125]
$AlCl_3$/[EMIm]Cl 1.3 : 1	12 mS cm^{-1} (ref. 98)	0 V to 2.35 V	120/100	2021 [109]
$AlCl_3$/caprolactam (1.85 : 1)–9.5% urea	—	0.5 V to 2.6 V	161/1000; 132/5000, 87% retention after 3000 cycles	2020 [124]
$AlCl_3$-TMAHCl 1.7 : 1	7.5 mS cm^{-1}	0.5 V to 2.4 V	134/2000, 167% retention after 3000 cycles	2020 [98]
$AlCl_3$/NaCl/KCl 61 : 26 : 13	—	0.5 V to 2.35 V	125/100, 90/4000, 100% retention after 300 cycles	2018 [128]
Gel polymer electrolytes				
$AlCl_3$/[EMIm]Cl–polyethylene oxide–SiO_2	13 mS cm^{-1}	0.5 V to 2.8 V	194/66	2024 [2]
$AlCl_3$/Et_3NHCl (2.0 : 1)–polyamide	0.15 mS cm^{-1}	0.8 V to 2.35 V	31/20	2023 [140]
$AlCl_3$/Et_3NHCl (1.7 : 1)–polyamide	3.86 mS cm^{-1}	1.0 V to 2.45 V	90/100; 94.6/200, % retention after 2000 cycles	2021 [139]
$AlCl_3$/[EMIm]Cl (1.3 : 1)–polyamide	6.61 mS cm^{-1}	1.0 V to 2.45 V	94/500, 98.9% retention after 4200 cycles	2021 [138]
$AlCl_3$/Et_3NHCl (1.7 : 1)–polyacrylamide	5.77 mS cm^{-1}	0.3 V to 2.3 V	91/1000, 97.8% retention after 800 cycles	2019 [136]

"—" means not mentioned.

performance are necessary. Key challenges that remain include limited rate capability, a lack of long-term cycling data, and poor interfacial compatibility under high-rate conditions.

Table 3 summarizes the various electrolytes reported for Al||graphite batteries over the years, including ionic liquids, deep eutectic electrolytes (DEEs), and gel polymer electrolytes. Among them, $AlCl_3$/[EMIm]Cl remains the most widely employed electrolyte due to its well-balanced electrochemical performance since 2015, and has been the benchmark system for AGDIBs. However, its practical application is hampered by critical drawbacks, such as high cost, corrosiveness, hygroscopicity, and high viscosity, which restrict material compatibility and limit rate performance, particularly under low-temperature conditions.

To address these limitations, a variety of alternative electrolytes have been investigated recent years, such as $AlCl_3$/urea, $AlCl_3$/acetamide, and $AlCl_3$/Et_3NHCl, as well as mixed ionic liquid systems. These systems generally offer reduced corrosiveness, lower cost, and improved safety, with some (*e.g.*, $AlCl_3$/urea) achieving ultralong cycling stability (>8000 cycles with 80% retention). In parallel, gel polymer electrolytes have emerged as promising solid-like electrolytes that mitigate leakage and corrosion. Although their ionic conductivities are generally lower than those of liquid systems, several formulations already deliver remarkable durability (>98% retention after 4000 cycles), highlighting their potential for safer and more robust AGDIBs.

Overall, as a benchmark electrolyte, $AlCl_3$/[EMIm]Cl offers balanced performance but suffers from high cost, strong corrosiveness, hygroscopicity, and high viscosity. Consequently, the development of cost-effective and less corrosive alternatives has become a key research priority.

- Alternative chloroaluminate electrolytes (*e.g.* $AlCl_3$/Et_3NHCl, $AlCl_3$/urea and its derivatives): show reduced toxicity and improved affordability, yet still face challenges in long-term stability and efficiency.
- Gel polymer electrolytes: enhance safety and structural integrity while achieving promising cycling stability, though the ionic conductivity remains relatively low.

Thus, developing cost-effective, less corrosive, and durable electrolytes that combine high ionic conductivity with long-term stability and mechanical robustness is essential for the practical advancement of AGDIB technology.

5. Other components

Other components include the current collector, separator, binder, and casing. The main challenge facing these components is their stability against corrosive electrolytes. To forge ahead with the development of AGDIBs, it is necessary to design and select proper cell components, especially for corrosive electrolyte systems.

5.1 Current collector

A current collector is an electrically conductive substrate to the cathode which is not free–standing. The selection of materials for current collector is limited to a few transition metals, semiconductors, and inert carbons, due to the strong corrosive imidazolium-based electrolytes. The onset of electrochemical oxidation for various current collectors from linear sweep voltammetry study is illustrated in Fig. 16a. The typical operating voltage window of 0.5 V to 2.4 V (*vs.* Al^{3+}/Al) is selected to balance electrode stability, electrolyte compatibility, and optimal electrochemical performance. The graphite cathode operates mainly within 1.5 V to 2.5 V, where anion intercalation (typically $AlCl_4^-$ or $Al_2Cl_7^-$) occurs. Within 0.5–2.4 V, zinc (Zn), tin (Sn), nickel (Ni), stainless steel (SS), titanium (Ti),

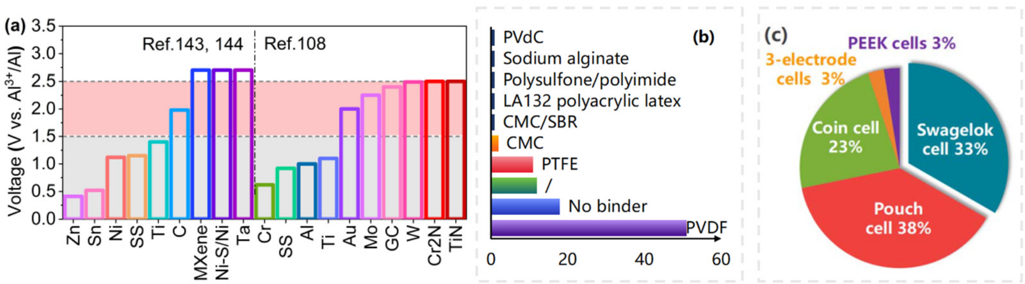

Fig. 16 (a) The oxidative stability, in terms of the voltage *versus* Al/Al^{3+}, of Ni–S/Ni,[143] MXene and other various current collector materials[144] in AlCl$_3$/[EMIm]Cl electrolyte with molar ratios of 1.3 (left) and 2.0 (right). Adapted from Wang, S. *et al.*, *Adv. Sci.*[108] Licensed under CC BY 4.0. ©2018 Wiley. (b) Number of publications reporting various binders used in AGDIBs based on literature survey ('/' indicates not mentioned). (c) Cell configurations applied in AGDIBs from the literature survey.

chromium (Cr) and Al can be easily oxidized by the acidic electrolyte during electrochemical testing. Carbon (C), gold (Au), molybdenum (Mo), and glassy carbon (GC) have relatively higher oxidation onset potentials vs Al^{3+}/Al but are still below the onset of electrolyte decomposition (typically 2.4–2.5 V vs Al^{3+}/Al). To date, Mo is the most widely used current collector (~53%), followed by Ni (~16%), carbon (~7%) and Tantalum (Ta) (~6%), according to literature. The stability of Mo is generally accepted owing to its high electrical conductivity (1.9×10^7 S m^{-1}). Nevertheless, Bamberg *et al.*[141] found that the instability of the molybdenum current collector resulted in increased capacity loss during self-discharge compared to glassy carbon, which was attributed to dissolved molybdenum species. Zemlyanushin *et al.*[142] further investigated the redox activity of Mo and its influence on electrochemical performance. From their study, three oxidation states of Mo (Mo^{4+}, Mo^{5+}, and Mo^{6+}) were observed on the Al anode electrode due to Mo-cation migration and adsorption. Coating the Mo current collector with electrochemically inactive Co_3O_4 suppresses Mo reactivity due to the reduced active Mo surface area. This highlights Mo's significant impact, which is non-negligible, as generally assumed, on the electrochemical performance.

Research focusing on current collectors is scarce, with less than ten publications identified. Given that Ni can be easily corroded in AlCl$_3$/[EMIm]Cl electrolyte, it is important to point out that it might not affect the cell performance since no electrochemical activity from Ni was observed in blank electrode tests.[4,82] A low-cost Ni–S/Ni current collector was made by electroplating amorphous Ni_3S_2 onto Ni foil using a scalable electrodeposition method.[143] Amorphous Ni_3S_2 has excellent flexibility, high oxidation potential (2.7 V) and conductivity (2.3×10^6 S m^{-1}) which are comparable to Ta current collectors (2.7 V, 8×10^6 S m^{-1}, respectively). A full cell with a Ni–S/Ni current collector shows similar long-term performance to the Ta current collector. Considering the high price of Ta, a Ni–S/Ni current collector can serve as an alternative. Wang *et al.*[108] fabricated a flexible current collector with an electrical conductivity of 4–4.5×10^6 S m^{-1} by magnetron sputtering titanium nitride (TiN) on polyimide substrates. Stable cathodic operation is observed at voltages of up to 2.5 V *versus* Al^{3+}/Al. The nitrogen atoms are believed to shield the underlying metal ions, protecting them from oxidation, which results in better stability than the pure metals. At a current density of 10 A g^{-1}, the power density is estimated to be 4500 W kg^{-1}. It is a highly promising alternative; however, the relatively complex synthesis has hindered its application beyond the initial study. Guan *et al.*[144] utilized MXene (Ti_3C_2Tx film) as a current collector. It indicates that the OH$^-$ and COO$^-$ groups incorporated onto the surface of Ti_3C_2Tx film could stop AlCl$_4^-$ ions from fully reaching the surface of the current collector, thus preventing the cathode materials from falling off the current collector because of its volume expansion. However, MXene materials have drawbacks, such as complex synthesis processes, sensitivity to air and moisture, and potential issues with electrolyte compatibility. Most importantly, MXenes exhibit high surface reactivity and can interact with metal components, such as aluminum, potentially leading to metal dissolution in the battery.

In summary, the stability of current collector is strongly influenced by the corrosive nature of electrolytes. Molybdenum is the most widely used due to its high conductivity and relative stability, though it can still undergo oxidation and contribute to capacity loss. Alternatives such as Ta, Ni–S/Ni, TiN-coated substrates, and MXene films offer promising conductivity and electrochemical stability, but each has trade-offs related to cost, synthesis complexity, or compatibility with electrolytes.

5.2 Separator

Glass fiber is mainly used as separators in AGDIBs, while very few studies have reported the use of polyacrylonitrile (PAN) and cellulose-based separators. Due to the low mechanical property and high thickness of glass fiber, it is challenging to realize practical applications. For optimal performance, a suitable separator should feature uniform porosity and thickness to prevent overheating, dendrite formation, and short circuits due to uneven cell operation. It should demonstrate good electrolyte wettability, be able to withstand the corrosive environment, and maintain proper mechanical properties.

According to available publications, only one research on separators was reported. A separator based on polyacrylonitrile (PAN) was fabricated by a simple electrospinning technique.[145]

In the $AlCl_3$/[EMIm]Cl (1.5 : 1) electrolyte, a highly uniform Al deposition was observed. When tested at a low current density of 25 mA g^{-1}, the battery employing a PAN separator achieved a specific capacity of 73.5 mAh g^{-1}, slightly outperforming the 68.4 mAh g^{-1} obtained with a glass fiber separator. Furthermore, the battery with the PAN separator demonstrated significantly enhanced performance at 50 °C compared to 25 °C under a higher current density of 200 mA g^{-1}. In this study, six commercially available separators were evaluated: (i) polypropylene (PP) monolayer, (ii) glass fibers, (iii) cellulose/PAN blended fibers, (iv) polyethylene (PE)/PP coated with poly(vinyl alcohol) (PVA), (v) open-structure PP micro- and nanofibers, and (vi) polyimide microfibers. These were immersed in the $AlCl_3$/[EMIm]Cl electrolyte for seven days to assess the chemical stability. Among them, only the glass fiber separator showed good compatibility, exhibiting minimal mass loss (1.2%) and no structural degradation. However, due to the limited data available on separator performance in AGDIBs, further systematic studies are needed. In summary, glass fiber is the most widely used and chemically compatible separator, though its low mechanical strength and high thickness limit practical applications. PAN-based separators, particularly those prepared *via* electrospinning, have shown promising performance, including uniform Al deposition and improved high-temperature stability, indicating strong potential for future development.

5.3 Binder

The cathode materials are generally coated onto a current collector with a polymer binder and carbon black as conductive agent except for free-standing and binder-free electrodes. In some cases, the volume expansion of the cathode from the intercalation of large-sized $AlCl_4^-$ can significantly weaken its attachment to the current collector, resulting in short cycling life.[144] A good binder should possess good adhesion and conductivity. It not only benefits the improvement of battery energy density, but also significantly reduces the internal resistance of the battery and has an important impact on the overall electrochemical performance. A survey shows that polyvinylidene fluoride (PVDF) is the most favored binder for cathode of AGDIBs, followed by polytetrafluoroethylene (PTFE), carboxymethyl cellulose (CMC), and other materials (Fig. 16b). In fact, the conventional PVDF binder dramatically reacts with $AlCl_3$/[EMIm]Cl electrolyte.[146] Dsoke and coworkers[147] compared the effect of PVDF binder in AGDIBs with polyvinylidene chloride (PVDC). Both PVDF and PVDC turned black after soaking in $AlCl_3$/[EMIm]Cl electrolyte, indicating that side reactions occurred. These reactions may lead to the formation of hydrofluoric acid (HF), which can damage the graphite structure and further exacerbate corrosion issues, ultimately contributing to capacity degradation. Interestingly, in contrast, electrodes using PVDF as a binder have also demonstrated larger cathode-specific capacities and improved rate capabilities.[148] These conflicting findings highlight the need for further investigation into the role of PVDF in such systems.

PTFE was reported to be insoluble in $AlCl_3$/[BMIM]Cl (mole ratio 1.1 : 1) electrolyte,[149] but its insolubility has not been confirmed in $AlCl_3$/[EMIm]Cl electrolyte. It is challenging to maintain consistent mass and thickness of the positive electrodes while using PTFE as a binder, which typically results in high mass loading. Additionally, a high graphite loading can lead to lower capacity, as the increased electrode volume hinders the smooth diffusion of $AlCl_4^-$ ions into the host material.[150] Nevertheless, the using PVDF or PTFE binders typically requires *N*-methylpyrrolidone (NMP), a solvent that is toxic and moisture-sensitive.[151] In contrast, water-soluble CMC and sodium alginate avoid NMP. These binders are low-cost, environmentally friendly, and demonstrate good thermal stability and long-term cycling stability. Rich in carboxyl and hydroxyl groups, they are expected to interact with functional groups on the surface of graphitic materials, forming an ideal gel phase network in the electrode. At the same time, polar/ionic interactions may occur between these functional groups and anions from electrolyte. Graphite electrodes using sodium alginate as the binder exhibited higher cycling stability compared to those based on PVDF at a current density of 1000 mA g^{-1}.[152] However, the solubility or potential side reactions of CMC and sodium alginate in $AlCl_3$/[EMIm]Cl electrolyte remain insufficiently studied and warrant further investigation. Overall, the choice of binder should be more critically examined in the future.

5.4 Casing

A variety of cell casings have been employed in AGDIBs, each with distinct advantages and limitations. As shown in Fig. 16c, Swagelok-type cells—typically composed of PTFE—are most used, followed by pouch cells, coin cells, and a small number of PEEK (polyether ether ketone) cells. Coin cells are favored for their compact design and suitability for mass production, but their stainless-steel structure is prone to corrosion in acidic electrolytes. Similarly, pouch cells, while enabling high cycling stability (up to 20 000 cycles[72]), use polypropylene liners that have been shown to corrode in Al-based electrolytes.[145] The long-term stability of this casing remains uncertain. Swagelok-type cells are ideal for lab-scale evaluations and closely mimic the environments of coin and pouch cells; however, their PTFE construction may suffer from corrosion, as fluorinated polymers are not always electrochemically inert.[153] Indeed, we found that initial cycling tests (100 cycles) revealed that Swagelok-type cells were less stable than coin cells. PEEK-based cells, though rarely used, offer promising features such as excellent corrosion resistance, high thermal stability, and mechanical durability, making them attractive for long-term cycling applications. Nevertheless, the high cost and manufacturing complexity of PEEK materials remain significant barriers to widespread adoption. In conclusion, while various casing materials offer specific benefits, none provide a fully optimal solution, highlighting the need for continued material innovation and systematic evaluation to ensure long-term stability and compatibility with corrosive electrolytes in AGDIB systems.

6. Summary and perspectives

In recent years, AGDIBs have attracted significant research interest, as Al stands out as a highly promising metallic anode due to its abundance, low cost, high theoretical capacity, and intrinsic safety. Despite these advantages, critical technical challenges associated with the anode, cathode, and electrolytes remain unresolved. This review has summarized recent progress in AGDIB development, analyzed the main obstacles, and discussed emerging strategies to address them. Based on these discussions, several future research directions can be outlined.

6.1 Al anode

Corrosion in aggressive electrolytes continues to destabilize the electrode–electrolyte interface, particularly during extended cycling, while dendrite formation can arise due to surface impurities, current density fluctuations, and the complex multi-step kinetics of Al plating/stripping. Surface modification strategies, such as the introduction of artificial Al_2O_3 layers, have shown potential to suppress corrosion and regulate deposition, but conflicting reports highlight their dual role in hindering Al dissolution or triggering localized pitting. Future efforts should prioritize a deeper mechanistic understanding of interfacial electrochemistry, with particular emphasis on the coupled evolution of passive films and SEI layers.

6.2 Carbon cathode

Graphitic carbon remains the most widely studied cathode material for AGDIBs, with $AlCl_4^-$ intercalation generally accepted as the primary storage mechanism. Graphite offers adaptable morphology and stable cycling, while few-layer graphene demonstrates exceptional rate performance and mechanical strength, making it particularly attractive for flexible devices. Hard carbons, especially those derived from biomass and doped with heteroatoms, deliver higher capacities at low current densities due to improved conductivity and expanded interlayer spacing. Future research should aim to balance crystalline order with structural optimization, guided by *in situ*/*operando* characterizations and theoretical modeling. Designing graphitic materials with carefully tuned interlayer spacing, well-controlled defect density, and strong mechanical integrity will be crucial for achieving higher capacities, improved rate performance, and long-term cycling stability in AGDIB cathodes.

6.3 Electrolytes and other components

Electrolytes play a decisive role in AGDIBs stability and performance yet remain a major bottleneck. Acidic electrolytes enable reversible Al plating/stripping but also induce severe corrosion of electrodes and other cell components such as current collectors, separators, and binders. While alternative casings (*e.g.*, Swagelok- and PEEK-based cells) can mitigate corrosion during laboratory testing, they are impractical for large-scale applications. Research has also shown that Cl-free non-corrosive electrolytes cannot currently sustain reversible Al electrochemistry, underscoring the trade-off between functionality and durability. Looking ahead, optimizing electrolyte formulations with controlled corrosiveness, combined with interface engineering to stabilize electrode–electrolyte interactions, will be essential. Parallel efforts to design corrosion-resistant cell components and integrate protective coatings can further extend device lifespan. Progress in these areas will be indispensable for bridging the gap between laboratory demonstrations and practical AGDIB deployment.

6.4 General outlook

Overall, the present understanding of charge/discharge mechanisms and interfacial processes in AGDIBs remains incomplete. Addressing these knowledge gaps through combined experimental and theoretical studies will be key. Moving forward, research priorities should include: (i) elucidating anode interfacial chemistry and SEI/passivation dynamics, (ii) optimizing defect and structure control in carbon cathodes, (iii) engineering electrolytes with a balance between functionality and corrosion resistance, and (iv) developing system-level strategies for improving the durability of all cell components. Progress along these directions will be crucial for unlocking the practical potential of AGDIBs in next-generation energy storage.

Conflicts of interest

The authors declare no conflict of interest.

Data availability

No new data were generated or analyzed in this study. All data discussed in this review are drawn from previously published sources, which are cited appropriately in the text and listed in the references.

Acknowledgements

The first author acknowledges the support from the China Scholarship Council.

References

1 S. Wang, *et al.*, Space limited growth strategy for ultrahigh areal capacity rechargeable aluminum batteries, *Energy Storage Mater.*, 2023, **60**, 102826, DOI: 10.1016/j.ensm.2023.102826.

2 O. M. Leung, *et al.*, Solid Polymer Electrolytes with Enhanced Electrochemical Stability for High–Capacity Aluminum Batteries, *Adv. Energy Mater.*, 2024, **14**, 2303285, DOI: 10.1002/aenm.202303285.

3 K. V. Kravchyk and M. V. Kovalenko, Rechargeable Dual–Ion Batteries with Graphite as a Cathode: Key Challenges and Opportunities, *Adv. Energy Mater.*, 2019, **9**, 1901749, DOI: 10.1002/aenm.201901749.

4 H. Chen, *et al.*, Ultrafast all-climate aluminum-graphene battery with quarter-million cycle life, *Sci. Adv.*, 2017, **3**, eaao723, DOI: 10.1126/sciadv.aao7233.

5 G. A. Elia, N. A. Kyeremateng, K. Marquardt and R. Hahn, An Aluminum/Graphite Battery with Ultra–High Rate Capability, *Batteries Supercaps*, 2018, **2**, 83–90, DOI: 10.1002/batt.201800114.

6 T. N. Pham-Truong, Q. Wang, J. Ghilane and H. Randriamahazaka, Recent Advances in the Development of Organic and Organometallic Redox Shuttles for Lithium-Ion Redox Flow Batteries, *ChemSusChem*, 2020, **13**, 2142–2159, DOI: 10.1002/cssc.201903379.

7 D. A. Elalfy, E. Gouda, M. F. Kotb, V. Bureš and B. E. Sedhom, Comprehensive review of energy storage systems technologies, objectives, challenges, and future trends, *Energy Strategy Rev.*, 2024, **54**, 101482, DOI: 10.1016/j.esr.2024.101482.

8 G. A. Ferrero, *et al.*, Solvent Co-Intercalation Reactions for Batteries and Beyond, *Chem. Rev.*, 2025, **125**, 3401–3439, DOI: 10.1021/acs.chemrev.4c00805.

9 M. Walter, M. Kovalenko and K. V. Kravchyk, Challenges and Benefits of Post-Lithium-ion Batteries, *New J. Chem.*, 2020, **44**, 1677–1683, DOI: 10.1039/C9NJ05682C.

10 M. Jiang, *et al.*, Challenges and Strategies of Low–Cost Aluminum Anodes for High–Performance Al–Based Batteries, *Adv. Mater.*, 2022, **34**, 2102026, DOI: 10.1002/adma.202102026.

11 J. Tu, *et al.*, Design Strategies of High-Performance Positive Materials for Nonaqueous Rechargeable Aluminum Batteries: From Crystal Control to Battery Configuration, *Small*, 2022, **18**, e2201362, DOI: 10.1002/smll.202201362.

12 X. Yang, *et al.*, Electrodeposition of aluminum from AlCl3-triethylamine hydrochloride ionic liquid, *Ionics*, 2025, **31**, 1655–1665, DOI: 10.1007/s11581-024-05989-1.

13 T. Jiang, C. M. J. Brym, G. Dubé, A. Lasia and G. M. Brisard, Electrodeposition of aluminium from ionic liquids: Part I—electrodeposition and surface morphology of aluminium from aluminium chloride (AlCl3)-1-ethyl-3-methylimidazolium chloride ([EMIm]Cl) ionic liquids, *Surf. Coat. Technol.*, 2006, **201**, 1–9, DOI: 10.1016/j.surfcoat.2005.10.046.

14 H. Go, M. R. Raj, Y. Tak and G. Lee, Electrochemically Surface–modified Aluminum Electrode Enabling High Performance and Ultra–long Cycling Life Al–ion Batteries, *Electroanalysis*, 2022, **34**, 1308–1317, DOI: 10.1002/elan.202100669.

15 P. Bhauriyal, A. Mahata and B. Pathak, The staging mechanism of AlCl(4) intercalation in a graphite electrode for an aluminium-ion battery, *Phys. Chem. Chem. Phys.*, 2017, **19**, 7980–7989, DOI: 10.1039/c7cp00453b.

16 J. Xu, *et al.*, Recent Progress in Graphite Intercalation Compounds for Rechargeable Metal (Li, Na, K, Al)-Ion Batteries, *Adv. Sci.*, 2017, **4**, 1700146, DOI: 10.1002/advs.201700146.

17 Z. Wang, *et al.*, Space-confined intercalation expansion strategy for simple and rapid synthesis of kish-based expanded graphite for aluminum ion batteries, *Carbon*, 2024, **223**, 119016, DOI: 10.1016/j.carbon.2024.119016.

18 M. C. Lin, *et al.*, An ultrafast rechargeable aluminium-ion battery, *Nature*, 2015, **520**, 325–328, DOI: 10.1038/nature14340.

19 S. Wang, K. V. Kravchyk, F. Krumeich and M. V. Kovalenko, Kish Graphite Flakes as a Cathode Material for an Aluminum Chloride-Graphite Battery, *ACS Appl. Mater. Interfaces*, 2017, **9**, 28478–28485, DOI: 10.1021/acsami.7b07499.

20 H. Xu, *et al.*, Low-cost AlCl3/Et3NHCl electrolyte for high-performance aluminum-ion battery, *Energy Storage Mater.*, 2019, **17**, 38–45, DOI: 10.1016/j.ensm.2018.08.003.

21 K. V. Kravchyk, C. Seno and M. V. Kovalenko, Limitations of Chloroaluminate Ionic Liquid Anolytes for Aluminum–Graphite Dual-Ion Batteries, *ACS Energy Lett.*, 2020, **5**, 545–549, DOI: 10.1021/acsenergylett.9b02832.

22 K. V. Kravchyk, S. Wang, L. Piveteau and M. V. Kovalenko, Efficient Aluminum Chloride–Natural Graphite Battery, *Chem. Mater.*, 2017, **29**, 4484–4492, DOI: 10.1021/acs.chemmater.7b01060.

23 S. Wang, *et al.*, A novel dual-graphite aluminum-ion battery, *Energy Storage Mater.*, 2018, **12**, 119–127, DOI: 10.1016/j.ensm.2017.12.010.

24 Z. Li, J. Liu, B. Niu, J. Li and F. Kang, A Novel Graphite-Graphite Dual Ion Battery Using an AlCl(3) -[EMIm]Cl Liquid Electrolyte, *Small*, 2018, **14**, e1800745, DOI: 10.1002/smll.201800745.

25 G. Razaz, *et al.*, Aluminum Alloy Anode with Various Iron Content Influencing the Performance of Aluminum-Ion Batteries, *Materials*, 2023, **16**, 933, DOI: 10.3390/ma16030933.

26 M. Bamberg, *et al.*, Insights into self-discharge processes of Al-graphite batteries, *Electrochim. Acta*, 2024, **488**, 144198, DOI: 10.1016/j.electacta.2024.144198.

27 D. Moser, *et al.*, Corrosion of Passive Aluminum Anodes in a Chloroaluminate Deep Eutectic Solvent for Secondary Batteries: The Bad, the Good, and the Ugly, *ACS Appl. Mater. Interfaces*, 2023, **15**, 882–892, DOI: 10.1021/acsami.2c16153.

28 L. Fan, H. Lu, J. Leng, Z. Sun and C. Chen, The effect of crystal orientation on the aluminum anodes of the aluminum–air batteries in alkaline electrolytes, *J. Power Sources*, 2015, **299**, 66–69, DOI: 10.1016/j.jpowsour.2015.08.095.

29 D. Lee, G. Lee and Y. Tak, Hypostatic instability of aluminum anode in acidic ionic liquid for aluminum-ion battery, *Nanotechnology*, 2018, **29**, 36LT01, DOI: 10.1088/1361-6528/aacd7f.

30 B. Long, *et al.*, Manipulating the corrosion homogeneity of aluminum anode toward long–life rechargeable alumi-

num battery, *Carbon Neutralization*, 2023, **3**, 64–73, DOI: 10.1002/cnl2.99.

31 S. Das, S. S. Manna and B. Pathak, Role of Additives in Solid Electrolyte Interphase Formation in Al Anode Dual-Ion Batteries, *ACS Appl. Energy Mater.*, 2022, **5**, 13398–13409, DOI: 10.1021/acsaem.2c02067.

32 Y. Xie, *et al.*, Optimized Electrode/Electrolyte Interface Engineering for Dendrite–Free Al Anode and Self–Activated Graphite Cathode, *Adv. Funct. Mater.*, 2024, **34**, 2411395, DOI: 10.1002/adfm.202411395.

33 Y. Xie, *et al.*, Dynamic molecular adsorption interface strategy for stable aluminum batteries, *Energy Storage Mater.*, 2024, **70**, 103545, DOI: 10.1016/j.ensm.2024.103545.

34 X. Li, X. Du and L. Xiong, Alkali assisted water treatment of aluminum promoting the growth of hydrated oxide film for energy conservation, *Surf. Interfaces*, 2023, **40**, 103039, DOI: 10.1016/j.surfin.2023.103039.

35 M. Guidat, *et al.*, In Situ Monitoring of the Al(110)–[EMImCl]:AlCl3 Interface by Reflection Anisotropy Spectroscopy, *Batteries Supercaps*, 2023, **7**, e202300394, DOI: 10.1002/batt.202300394.

36 F. Rahide, *et al.*, Modification of Al Surface via Acidic Treatment and its Impact on Plating and Stripping, *ChemSusChem*, 2024, **17**, e202301142, DOI: 10.1002/cssc.202301142.

37 D.-M. She, *et al.*, Surface Evolution of Aluminum Electrodes in Non-Aqueous Aluminum Batteries, *J. Electrochem. Soc.*, 2020, **167**, 130530, DOI: 10.1149/1945-7111/abbb09.

38 H. Chen, *et al.*, Oxide Film Efficiently Suppresses Dendrite Growth in Aluminum-Ion Battery, *ACS Appl. Mater. Interfaces*, 2017, **9**, 22628–22634, DOI: 10.1021/acsami.7b07024.

39 S. Choi, H. Go, G. Lee and Y. Tak, Electrochemical properties of an aluminum anode in an ionic liquid electrolyte for rechargeable aluminum-ion batteries, *Phys. Chem. Chem. Phys.*, 2017, **19**, 8653–8656, DOI: 10.1039/c6cp08776k.

40 L. C. Loaiza, N. Lindahl and P. Johansson, Initial Evolution of Passivation Layers in Non-Aqueous Aluminium Batteries, *J. Electrochem. Soc.*, 2023, **170**, 030512, DOI: 10.1149/1945-7111/acb108.

41 R. Böttcher, S. Mai, A. Ispas and A. Bund, Aluminum Deposition and Dissolution in [EMIm]Cl-Based Ionic Liquids–Kinetics of Charge–Transfer and the Rate–Determining Step, *J. Electrochem. Soc.*, 2020, **167**, 102516, DOI: 10.1149/1945-7111/ab9c84.

42 B. Craig, T. Schoetz, A. Cruden and C. Ponce de Leon, Review of current progress in non-aqueous aluminium batteries, *Renewable Sustainable Energy Rev.*, 2020, **133**, 110100, DOI: 10.1016/j.rser.2020.110100.

43 G. A. Elia, *et al.*, Insights into the reversibility of aluminum graphite batteries, *J. Mater. Chem. A*, 2017, **5**, 9682–9690, DOI: 10.1039/c7ta01018d.

44 D. Muñoz-Torrero, *et al.*, Investigation of different anode materials for aluminium rechargeable batteries, *J. Power Sources*, 2018, **374**, 77–83, DOI: 10.1016/j.jpowsour.2017.11.032.

45 S. Wang, *et al.*, Preferred crystal plane electrodeposition of aluminum anode with high lattice-matching for long-life aluminum batteries, *Nat. Commun.*, 2024, **15**, 6476, DOI: 10.1038/s41467-024-50723-0.

46 N. Sabi, *et al.*, Surface Properties–Performance Relationship of Aluminum Foil as Negative Electrode for Rechargeable Aluminum Batteries, *Batteries Supercaps*, 2023, **6**, e202300298, DOI: 10.1002/batt.202300298.

47 W. Liu, *et al.*, Surficial modification enabling planar Al growth toward dendrite-free metal anodes for rechargeable aluminum batteries, *Sci. China: Chem.*, 2024, **67**, 1341–1351, DOI: 10.1007/s11426-023-1940-1.

48 S. Wang, *et al.*, Stable aluminum metal anodes with high ionic conductivity and high aluminophilic site, *Chem. Eng. J.*, 2024, **494**, 153194, DOI: 10.1016/j.cej.2024.153194.

49 S. Wang, *et al.*, Bottom growth strategy for high areal capacity rechargeable aluminum batteries, *Nano Energy*, 2023, **114**, 108626, DOI: 10.1016/j.nanoen.2023.108626.

50 M. Guo, *et al.*, High performance aluminum foam-graphite dual-ion batteries and failure analysis, *J. Alloys Compd.*, 2020, **838**, 155640, DOI: 10.1016/j.jallcom.2020.155640.

51 X. Tong, *et al.*, Core–Shell Aluminum@Carbon Nanospheres for Dual–Ion Batteries with Excellent Cycling Performance under High Rates, *Adv. Energy Mater.*, 2018, **8**, 1701967, DOI: 10.1002/aenm.201701967.

52 P. Qin, *et al.*, Bubble–Sheet–Like Interface Design with an Ultrastable Solid Electrolyte Layer for High–Performance Dual–Ion Batteries, *Adv. Mater.*, 2017, **29**, 1606805, DOI: 10.1002/adma.201606805.

53 X. Tong, F. Zhang, B. Ji, M. Sheng and Y. Tang, Carbon–Coated Porous Aluminum Foil Anode for High–Rate, Long–Term Cycling Stability, and High Energy Density Dual–Ion Batteries, *Adv. Mater.*, 2016, **28**, 9979–9985, DOI: 10.1002/adma.201603735.

54 C. Tan, *et al.*, Different technology packages for aluminium smelters worldwide to deliver the 1.5 °C target, *Nat. Clim. Change*, 2025, **15**, 51–58, DOI: 10.1038/s41558-024-02193-x.

55 S. Al-Alimi, *et al.*, Recycling aluminium for sustainable development: A review of different processing technologies in green manufacturing, *Results Eng.*, 2024, **23**, 102566, DOI: 10.1016/j.rineng.2024.102566.

56 E. Fuentes-Mendoza, *et al.*, Navigating the Challenges of Rechargeable Aluminum Battery Research: Material Instabilities, Technical Hurdles, and Future Directions, *ChemElectroChem*, 2025, **12**, e202400705, DOI: 10.1002/celc.202400705.

57 Y. Wang, Z. Zhang, F. Yuan and B. Wang, Design and modification of carbon-based materials for high energy density non-aqueous aluminum ion batteries: A review, *J. Power Sources*, 2024, **597**, 234110, DOI: 10.1016/j.jpowsour.2024.234110.

58 J. H. Xu, D. E. Turney, A. L. Jadhav and R. J. Messinger, Effects of Graphite Structure and Ion Transport on the

Electrochemical Properties of Rechargeable Aluminum–Graphite Batteries, *ACS Appl. Energy Mater.*, 2019, **2**, 7799–7810, DOI: 10.1021/acsaem.9b01184.

59 L. Wang, *et al.*, Graphite recycling from spent lithium-ion batteries for fabrication of high-performance aluminum-ion batteries, *Rare Met.*, 2024, **43**, 2161–2171, DOI: 10.1007/s12598-023-02572-x.

60 D. Y. Wang, *et al.*, Advanced rechargeable aluminium ion battery with a high-quality natural graphite cathode, *Nat. Commun.*, 2017, **8**, 14283, DOI: 10.1038/ncomms14283.

61 Z. Wang, *et al.*, Application of purified kish flake graphite as a potential cathode material for high-performance aluminum ion batteries, *J. Alloys Compd.*, 2023, **954**, 170197, DOI: 10.1016/j.jallcom.2023.170197.

62 Y. Wu, *et al.*, 3D Graphitic Foams Derived from Chloroaluminate Anion Intercalation for Ultrafast Aluminum-Ion Battery, *Adv. Mater.*, 2016, **28**, 9218–9222, DOI: 10.1002/adma.201602958.

63 D. Muñoz-Torrero, A. Molina, J. Palma, E. Ventosa and R. Marcilla, Widely commercial carbonaceous materials as cathode for Al-ion batteries, *Carbon*, 2020, **167**, 475–484, DOI: 10.1016/j.carbon.2020.06.019.

64 W.-L. Song, *et al.*, Cellulose-derived flake graphite as positive electrodes for Al-ion batteries, *Sustainable Energy Fuels*, 2019, **3**, 3561–3568, DOI: 10.1039/c9se00656g.

65 J. Tu, *et al.*, High-efficiency transformation of amorphous carbon into graphite nanoflakes for stable aluminum-ion battery cathodes, *Nanoscale*, 2019, **11**, 12537–12546, DOI: 10.1039/c9nr03112j.

66 C. Zhang, *et al.*, Amorphous Carbon-Derived Nanosheet-Bricked Porous Graphite as High-Performance Cathode for Aluminum-Ion Batteries, *ACS Appl. Mater. Interfaces*, 2018, **10**, 26510–26516, DOI: 10.1021/acsami.8b07590.

67 X. Dong, *et al.*, A graphitized expanded graphite cathode for aluminum-ion battery with excellent rate capability, *J. Energy Chem.*, 2022, **66**, 38–44, DOI: 10.1016/j.jechem.2021.07.016.

68 S. Jiao, *et al.*, An industrialized prototype of the rechargeable Al/AlCl 3 -[EMIm]Cl/graphite battery and recycling of the graphitic cathode into graphene, *Carbon*, 2016, **109**, 276–281, DOI: 10.1016/j.carbon.2016.08.027.

69 Z. Liu, *et al.*, Carbon Nanoscrolls for Aluminum Battery, *ACS Nano*, 2018, **12**, 8456–8466, DOI: 10.1021/acsnano.8b03961.

70 L. Hou, *et al.*, Electrochemical Performance of Graphitic Multi-walled Carbon Nanotubes with Different Aspect Ratios as Cathode Materials for Aluminum-ion Batteries, *ChemistryOpen*, 2020, **9**, 812–817, DOI: 10.1002/open.202000166.

71 H. Yoon, *et al.*, Chloroaluminate Anion Intercalation in Graphene and Graphite: From Two-Dimensional Devices to Aluminum-Ion Batteries, *Nano Lett.*, 2022, **22**, 1726–1733, DOI: 10.1021/acs.nanolett.1c04832.

72 Q. Zhang, *et al.*, Low-temperature synthesis of edge-rich graphene paper for high-performance aluminum batteries, *Energy Storage Mater.*, 2018, **15**, 361–367, DOI: 10.1016/j.ensm.2018.06.021.

73 X. Yu, B. Wang, D. Gong, Z. Xu and B. Lu, Graphene Nanoribbons on Highly Porous 3D Graphene for High-Capacity and Ultrastable Al-Ion Batteries, *Adv. Mater.*, 2017, **29**, 1604118, DOI: 10.1002/adma.201604118.

74 W. Guan, *et al.*, Stable Low–Temperature Al Batteries Enabled by Integrating Polydopamine–Derived N–Doped Carbon Nanospheres With Flake Graphite, *Small*, 2023, **20**, 2303836, DOI: 10.1002/smll.202303836.

75 A. Childress, *et al.*, Effect of nitrogen doping in the few layer graphene cathode of an aluminum ion battery, *Chem. Phys. Lett.*, 2019, **733**, 136669, DOI: 10.1016/j.cplett.2019.136669.

76 A. S. Childress, P. Parajuli, J. Zhu, R. Podila and A. M. Rao, A Raman spectroscopic study of graphene cathodes in high-performance aluminum ion batteries, *Nano Energy*, 2017, **39**, 69–76, DOI: 10.1016/j.nanoen.2017.06.038.

77 H. Chen, *et al.*, A Defect-Free Principle for Advanced Graphene Cathode of Aluminum-Ion Battery, *Adv. Mater.*, 2017, **29**, 1605958, DOI: 10.1002/adma.201605958.

78 H. Chen, *et al.*, High–Quality Graphene Microflower Design for High–Performance Li–S and Al–Ion Batteries, *Adv. Energy Mater.*, 2017, **7**, 1700051, DOI: 10.1002/aenm.201700051.

79 P. Almodóvar, *et al.*, Enhancing Aluminium–Ion Battery Performance with Carbon Xerogel Cathodes, *Batteries Supercaps*, 2024, **7**, e202400114, DOI: 10.1002/batt.202400114.

80 S. Li, Z. Zhang, F. Yuan, Z. Wang and B. Wang, Balancing interlayer spacing, pore structures and conductivity endows hard carbon with high capacity for rechargeable aluminum batteries, *Phys. Chem. Chem. Phys.*, 2024, **26**, 16838–16846, DOI: 10.1039/d4cp01415d.

81 J. Li, *et al.*, Pseudocapacitive Heteroatom–Doped Carbon Cathode for Aluminum–Ion Batteries with Ultrahigh Reversible Stability, *Energy Environ. Mater.*, 2024, **7**, e12733, DOI: 10.1002/eem2.12733.

82 C. Li, *et al.*, Heteroatomic interface engineering in MOF-derived carbon heterostructures with built-in electric-field effects for high performance Al-ion batteries, *Energy Environ. Sci.*, 2018, **11**, 3201–3211, DOI: 10.1039/c8ee01046c.

83 D. D. L. Chung, Review Graphite, *J. Mater. Sci.*, 2002, **37**, 1475–1489, DOI: 10.1023/A:1014915307738.

84 J. V. Rani, V. Kanakaiah, T. Dadmal, M. S. Rao and S. Bhavanarushi, Fluorinated Natural Graphite Cathode for Rechargeable Ionic Liquid Based Aluminum–Ion Battery, *J. Electrochem. Soc.*, 2013, **160**, A1781–A1784, DOI: 10.1149/2.072310jes.

85 H. Sun, *et al.*, A new aluminium-ion battery with high voltage, high safety and low cost, *Chem. Commun.*, 2015, **51**, 11892–11895, DOI: 10.1039/c5cc00542f.

86 G. Greco, *et al.*, Influence of the electrode nano/microstructure on the electrochemical properties of graphite in

aluminum batteries, *J. Mater. Chem. A*, 2018, **6**, 22673–22680, DOI: 10.1039/c8ta08319c.

87 D.-Y. Wang, *et al.*, Insights into dynamic molecular intercalation mechanism for Al C battery by operando synchrotron X-ray techniques, *Carbon*, 2019, **146**, 528–534, DOI: 10.1016/j.carbon.2019.01.038.

88 J. H. Xu, A. L. Jadhav, D. E. Turney and R. J. Messinger, Molecular-level environments of intercalated chloroaluminate anions in rechargeable aluminum-graphite batteries revealed by solid-state NMR spectroscopy, *J. Mater. Chem. A*, 2020, **8**, 16006–16017, DOI: 10.1039/d0ta02611e.

89 G. A. Elia, *et al.*, Simultaneous X-Ray Diffraction and Tomography Operando Investigation of Aluminum/Graphite Batteries, *Adv. Funct. Mater.*, 2020, **30**, 2003913, DOI: 10.1002/adfm.202003913.

90 M. Zhang, X. Song, X. Ou and Y. Tang, Rechargeable batteries based on anion intercalation graphite cathodes, *Energy Storage Mater.*, 2019, **16**, 65–84, DOI: 10.1016/j.ensm.2018.04.023.

91 C. J. Pan, *et al.*, An operando X-ray diffraction study of chloroaluminate anion-graphite intercalation in aluminum batteries, *Proc. Natl. Acad. Sci. U. S. A.*, 2018, **115**, 5670–5675, DOI: 10.1073/pnas.1803576115.

92 G. Greco, G. A. Elia, D. Hermida-Merino, R. Hahn and S. Raoux, A Direct Real-Time Observation of Anion Intercalation in Graphite Process and Its Fully Reversibility by SAXS/WAXS Techniques, *Small Methods*, 2023, **7**, e2201633, DOI: 10.1002/smtd.202201633.

93 M. Angell, *et al.*, High Coulombic efficiency aluminum-ion battery using an AlCl3-urea ionic liquid analog electrolyte, *Proc. Natl. Acad. Sci. U. S. A.*, 2017, **114**, 834–839, DOI: 10.1073/pnas.1619795114.

94 S. Agrawal, *et al.*, Temperature-insensitive fast anion intercalation kinetics in graphite electrodes for aluminum-ion batteries, *Electrochim. Acta*, 2022, **428**, 140892, DOI: 10.1016/j.electacta.2022.140892.

95 Z. Li, J. Li, X. Li and W. Zhang, Pseudocapacitance effect in Al-C batteries with expanded graphite positive electrode at different temperatures, *J. Power Sources*, 2020, **467**, 228323, DOI: 10.1016/j.jpowsour.2020.228323.

96 Z. Wang, D. Zhang, J. Chen, R. Hong and M. Li, High-performance aluminum-ion batteries enabled by architected reduced graphene oxide electrodes, *Surf. Interfaces*, 2025, **63**, 106348, DOI: 10.1016/j.surfin.2025.106348.

97 C. An, *et al.*, Electrostatic modification of expanded graphite cathode for high-performance aluminum-ion batteries, *J. Electroanal. Chem.*, 2023, **947**, 117761, DOI: 10.1016/j.jelechem.2023.117761.

98 K. L. Ng, T. Dong, J. Anawati and G. Azimi, High–Performance Aluminum Ion Battery Using Cost–Effective AlCl3–Trimethylamine Hydrochloride Ionic Liquid Electrolyte, *Adv. Sustainable Syst.*, 2020, **4**, 2000074, DOI: 10.1002/adsu.202000074.

99 B. Wang, *et al.*, Synergistic effect of pore structure and crystalline domains enabling high capacity toward non-aqueous rechargeable aluminum batteries, *J. Phys. Chem. Solids*, 2023, **179**, 111394, DOI: 10.1016/j.jpcs.2023.111394.

100 P. Thanwisai, *et al.*, Mesoporous and defective activated carbon cathode for AlCl4− anion storage in non-aqueous aluminium-ion batteries, *Carbon*, 2022, **191**, 195–204, DOI: 10.1016/j.carbon.2022.01.063.

101 O. M. Leung, T. Schoetz, T. Prodromakis and C. Ponce de Leon, Review—Progress in Electrolytes for Rechargeable Aluminium Batteries, *J. Electrochem. Soc.*, 2021, **168**, 056509, DOI: 10.1149/1945-7111/abfb36.

102 C. Ferrara, V. Dall'Asta, V. Berbenni, E. Quartarone and P. Mustarelli, Physicochemical characterization of AlCl3–1-ethyl-3-methylimidazolium chloride ionic liquid electrolytes for aluminum rechargeable batteries, *J. Phys. Chem. C*, 2017, **121**, 26607–26614, DOI: 10.1021/acs.jpcc.7b07562.

103 R. Revel, T. Audichon and S. Gonzalez, Non-aqueous aluminium–air battery based on ionic liquid electrolyte, *J. Power Sources*, 2014, **272**, 415–421, DOI: 10.1016/j.jpowsour.2014.08.056.

104 H. M. Chakrabarti, *et al.*, Prospects of applying ionic liquids and deep eutectic solvents for renewable energy storage by means of redox flow batteries, *Renewable Sustainable Energy Rev.*, 2014, **30**, 254–270, DOI: 10.1016/j.rser.2013.10.004.

105 S. S. Manna, Identifying suitable ionic liquid electrolytes for al dual–ion batteries: role of electrochemical window, conductivity and voltage, *Mater. Adv.*, 2020, **1**, 1354–1363, DOI: 10.1039/d0ma00292e.

106 T. Schoetz, C. P. de Leon, M. Ueda and A. Bund, Perspective—State of the Art of Rechargeable Aluminum Batteries in Non-Aqueous Systems, *J. Electrochem. Soc.*, 2017, **164**, A3499–A3502, DOI: 10.1149/2.0311714jes.

107 M. R. Palacin, *et al.*, Roadmap on multivalent batteries, *J. Phys.: Energy*, 2024, **6**, 031501, DOI: 10.1088/2515-7655/ad34fc.

108 S. Wang, *et al.*, Aluminum Chloride-Graphite Batteries with Flexible Current Collectors Prepared from Earth-Abundant Elements, *Adv. Sci.*, 2018, **5**, 1700712, DOI: 10.1002/advs.201700712.

109 S. Wang, M. V. Kovalenko and K. V. Kravchyk, AlCl3−Saturated Ionic Liquid Anolyte with an Excess of AlCl3 for Al–Graphite Dual–Ion Batteries, *Batteries Supercaps*, 2021, **4**, 929–933, DOI: 10.1002/batt.202000289.

110 C.-H. Tseng, *et al.*, Corrosion behaviors of materials in aluminum chloride–1-ethyl-3-methylimidazolium chloride ionic liquid, *Electrochem. Commun.*, 2010, **12**, 1091–1094, DOI: 10.1016/j.elecom.2010.05.036.

111 V. A. Elterman, *et al.*, Chloroaluminate ionic liquids for low-temperature aluminum-ion batteries, *J. Mol. Liq.*, 2024, **394**, 123702, DOI: 10.1016/j.molliq.2023.123702.

112 V. A. Elterman, P. Y. Shevelin, L. A. Yolshina and A. V. Borozdin, Electrodeposition of aluminium from the chloroaluminate ionic liquid 1-ethyl-3-methylimidazolium chloride, *Electrochim. Acta*, 2021, **389**, 138715, DOI: 10.1016/j.electacta.2021.138715.

113 V. A. Elterman, P. Y. Shevelin, L. A. Yolshina and A. V. Borozdin, Features of aluminum electrodeposition from 1,3-dialkylimidazolium chloride chloroaluminate ionic liquids, *J. Mol. Liq.*, 2022, **351**, 118693, DOI: 10.1016/j.molliq.2022.118693.

114 T. Schoetz, J. H. Xu and R. J. Messinger, Ionic Liquid Electrolytes with Mixed Organic Cations for Low-Temperature Rechargeable Aluminum–Graphite Batteries, *ACS Appl. Energy Mater.*, 2023, **6**, 2845–2854, DOI: 10.1021/acsaem.2c03762.

115 F. Gan, *et al.*, Low cost ionic liquid electrolytes for rechargeable aluminum/graphite batteries, *Ionics*, 2019, **25**, 4243–4249, DOI: 10.1007/s11581-019-02983-w.

116 C. Mukundan, M. Eckert and J. F. Drillet, Impact of Aluminium Electrode Potential during Charging on Aluminium–Ion Battery Performance with TEA–AlCl3 Electrolyte, *Batteries Supercaps*, 2023, **6**, e202300042, DOI: 10.1002/batt.202300042.

117 X. Dong, *et al.*, Commercial expanded graphite as high-performance cathode for low-cost aluminum-ion battery, *Carbon*, 2019, **148**, 134–140, DOI: 10.1016/j.carbon.2019.03.080.

118 K. L. Ng, *et al.*, A low-cost rechargeable aluminum/natural graphite battery utilizing urea-based ionic liquid analog, *Electrochim. Acta*, 2019, **327**, 135031, DOI: 10.1016/j.electacta.2019.135031.

119 M. Angell, G. Zhu, M. C. Lin, Y. Rong and H. Dai, Ionic Liquid Analogs of AlCl3 with Urea Derivatives as Electrolytes for Aluminum Batteries, *Adv. Funct. Mater.*, 2019, **30**, 1901928, DOI: 10.1002/adfm.201901928.

120 H. Jiao, C. Wang, J. Tu, D. Tian and S. Jiao, A rechargeable Al-ion battery: Al/molten AlCl(3)-urea/graphite, *Chem. Commun.*, 2017, **53**, 2331–2334, DOI: 10.1039/c6cc09825h.

121 J. Li, J. Tu, H. Jiao, C. Wang and S. Jiao, Ternary AlCl3-Urea-[EMIm]Cl Ionic Liquid Electrolyte for Rechargeable Aluminum-Ion Batteries, *J. Electrochem. Soc.*, 2017, **164**, A3093–A3100, DOI: 10.1149/2.0811713jes.

122 T. Tsuda, R. Miyakawa and S. Kuwabata, Aluminum Nanoplatelet Electrodeposition in AlCl3–1-Ethyl-3-Methylimidazolium Chloride–Urea Melts, *J. Electrochem. Soc.*, 2022, **169**, 092520, DOI: 10.1149/1945-7111/ac91fc.

123 J. Wang, T. Schoetz, L. W. Gordon, E. J. Biddinger and R. J. Messinger, Ternary Ionic Liquid Analogues as Electrolytes for Ambient and Low-Temperature Rechargeable Aluminum Batteries, *ACS Appl. Energy Mater.*, 2024, **7**, 5438–5446, DOI: 10.1021/acsaem.4c00739.

124 C. Xu, *et al.*, High-performance aluminum-ion batteries based on AlCl3/caprolactam electrolytes, *Sustainable Energy Fuels*, 2020, **4**, 121–127, DOI: 10.1039/c9se00941h.

125 F. Jach, *et al.*, A Low–Cost Al–Graphite Battery with Urea and Acetamide–Based Electrolytes, *ChemElectroChem*, 2021, **8**, 1988–1992, DOI: 10.1002/celc.202100183.

126 W. Chu, *et al.*, High–Voltage Deep Eutectic Solvent Electrolyte with Fluorine–Substituted Acetamide Additive for Aluminum–ion Battery, *Adv. Funct. Mater.*, 2023, **34**, 2305194, DOI: 10.1002/adfm.202305194.

127 X. Bao, *et al.*, A deep eutectic electrolyte of AlCl3−acetamide for rechargeable aluminum-ion batteries, *New J. Chem.*, 2024, **48**, 5893–5901, DOI: 10.1039/d4nj00147h.

128 C. Y. Chen, T. Tsuda, S. Kuwabata and C. L. Hussey, Rechargeable aluminum batteries utilizing a chloroaluminate inorganic ionic liquid electrolyte, *Chem. Commun.*, 2018, **54**, 4164–4167, DOI: 10.1039/c8cc00113h.

129 F. Rahide, E. Zemlyanushin, G.-M. Bosch and S. Dsoke, Open Challenges on Aluminum Triflate-Based Electrolytes for Aluminum Batteries, *J. Electrochem. Soc.*, 2023, **170**, 030546, DOI: 10.1149/1945-7111/acc762.

130 F. Rahide, *et al.*, Hindered Aluminum Plating and Stripping in Urea/NMA/Al(OTF)3 as a Cl-Free Electrolyte for Aluminum Batteries, *J. Electrochem. Soc.*, 2023, **170**, 120534, DOI: 10.1149/1945-7111/ad1553.

131 M. Talari, *et al.*, Exploring the possibility of aluminum plating/stripping from a non–corrosive Al(OTf)3–based electrolyte, *Batteries Supercaps*, 2024, **8**, e202400317, DOI: 10.1002/batt.202400317.

132 H. Wang, *et al.*, High-Voltage and Noncorrosive Ionic Liquid Electrolyte Used in Rechargeable Aluminum Battery, *ACS Appl. Mater. Interfaces*, 2016, **8**, 27444–27448, DOI: 10.1021/acsami.6b10579.

133 P. Meng, *et al.*, Air-Stable Binary Hydrated Eutectic Electrolytes with Unique Solvation Structure for Rechargeable Aluminum-Ion Batteries, *Nano-Micro Lett.*, 2023, **15**, 188, DOI: 10.1007/s40820-023-01160-z.

134 X. G. Sun, *et al.*, Polymer gel electrolytes for application in aluminum deposition and rechargeable aluminum ion batteries, *Chem. Commun.*, 2016, **52**, 292–295, DOI: 10.1039/c5cc06643c.

135 Z. Yu, *et al.*, Flexible Stable Solid–State Al–Ion Batteries, *Adv. Funct. Mater.*, 2018, **29**, 1806799, DOI: 10.1002/adfm.201806799.

136 Z. Yu, *et al.*, Gel electrolytes with a wide potential window for high-rate Al-ion batteries, *J. Mater. Chem. A*, 2019, **7**, 20348–20356, DOI: 10.1039/c9ta06815e.

137 T. Schoetz, O. Leung, C. P. de Leon, C. Zaleski and I. Efimov, Aluminium Deposition in EMImCl-AlCl3 Ionic Liquid and Ionogel for Improved Aluminium Batteries, *J. Electrochem. Soc.*, 2020, **167**, 040516, DOI: 10.1149/1945-7111/ab7573.

138 Z. Liu, *et al.*, A reliable gel polymer electrolyte enables stable cycling of rechargeable aluminum batteries in a wide-temperature range, *J. Power Sources*, 2021, **497**, 229839, DOI: 10.1016/j.jpowsour.2021.229839.

139 Z. Liu, *et al.*, Low-Cost Gel Polymer Electrolyte for High-Performance Aluminum-Ion Batteries, *ACS Appl. Mater. Interfaces*, 2021, **13**, 28164–28170, DOI: 10.1021/acsami.1c05476.

140 A. Mohammad, T. Köhler, S. Biswas, H. Stöcker and D. C. Meyer, A Flexible Solid-State Ionic Polymer Electrolyte for Application in Aluminum Batteries, *ACS Appl. Energy Mater.*, 2023, **6**, 2914–2923, DOI: 10.1021/acsaem.2c03906.

141 M. Bamberg, *et al.*, Insights into self-discharge processes of Al-graphite batteries, *Electrochim. Acta*, 2024, **488**, 144198, DOI: 10.1016/j.electacta.2024.144198.

142 E. Zemlyanushin, B. Schwarz and S. Dsoke, Dissolution of molybdenum current collector as Crucial and Undesired process in aluminum batteries, *J. Power Sources*, 2025, **633**, 236458, DOI: 10.1016/j.jpowsour.2025.236458.

143 H. Guo, R. Zhou, X. Li, Z. Li and S. Liu, Surface amorphous coating for an economical and high-stability current collector for rechargeable aluminum-ion batteries, *Nanotechnology*, 2022, **33**, 248001, DOI: 10.1088/1361-6528/ac5287.

144 W. Guan, *et al.*, The Negative-Charge-Triggered "Dead Zone" between Electrode and Current Collector Realizes Ultralong Cycle Life of Aluminum-Ion Batteries, *Adv. Mater.*, 2023, **35**, e2205489, DOI: 10.1002/adma.202205489.

145 G. A. Elia, *et al.*, Polyacrylonitrile Separator for High-Performance Aluminum Batteries with Improved Interface Stability, *ACS Appl. Mater. Interfaces*, 2017, **9**, 38381–38389, DOI: 10.1021/acsami.7b09378.

146 Y. Uemura, *et al.*, Graphene Nanoplatelet Composite Cathode for a Chloroaluminate Ionic Liquid-Based Aluminum Secondary Battery, *ACS Appl. Energy Mater.*, 2018, **1**, 2269–2274, DOI: 10.1021/acsaem.8b00341.

147 E. Zemlyanushin, A. L. Müller, T. Tsuda and S. Dsoke, Side-Reactions of Polyvinylidene Fluoride and Polyvinylidene Chloride Binders with Aluminum Chloride-Based Ionic Liquid Electrolyte in Rechargeable Aluminum-Batteries, *J. Electrochem. Soc.*, 2024, **171**, 110507, DOI: 10.1149/1945-7111/ad8a93.

148 J. Yu, *et al.*, Pencil-Drawing Graphite Nanosheets: A Simple and Effective Cathode for High-Capacity Aluminum Batteries, *Small Methods*, 2022, **6**, 2200026, DOI: 10.1002/smtd.202200026.

149 H. Wang, *et al.*, Binder-Free V2O5 Cathode for Greener Rechargeable Aluminum Battery, *ACS Appl. Mater. Interfaces*, 2015, **7**, 80–84, DOI: 10.1021/am508001h.

150 M.-C. Huang, *et al.*, Influence of High Loading on the Performance of Natural Graphite-Based Al Secondary Batteries, *Energies*, 2018, **11**, 2760.

151 T. Qin, H. Yang, Q. Li, X. Yu and H. Li, Design of functional binders for high-specific-energy lithium-ion batteries: from molecular structure to electrode properties, *Ind. Chem. Mater.*, 2024, **2**, 191–225, DOI: 10.1039/d3im00089c.

152 Z. Yang, *et al.*, Aqueous Binders Compatible with Ionic Liquid Electrolyte for High-Performance Aluminum-Ion Batteries, *Chem. – Eur. J.*, 2023, **29**, e202203546, DOI: 10.1002/chem.202203546.

153 J. Shi, J. Zhang and J. Guo, Avoiding Pitfalls in Rechargeable Aluminum Batteries Research, *ACS Energy Lett.*, 2019, **4**, 2124–2129, DOI: 10.1021/acsenergylett.9b01285.